

AFRL-ML-WP-TR-1998-4105

**ON MICROSTRUCTURAL THEORY OF PLASTIC DEFORMATION
IN FACE-CENTERED-CUBIC MATERIALS**



**RONALD L. BAGLEY
CALLIE C. BAST
THE UNIVERSITY OF TEXAS AT SAN ANTONIO**

**DAVID L. CRANE
LOS ALAMOS, NEW MEXICO**

FINAL REPORT FOR JULY 1996 THROUGH OCTOBER 1997

APPROVED FOR PUBLIC RELEASE; DISTRIBUTION IS UNLIMITED

**"THE VIEWS AND CONCLUSIONS CONTAINED HEREIN ARE THOSE OF THE
AUTHORS AND SHOULD NOT BE INTERPRETED AS NECESSARILY REPRESENTING
THE OFFICIAL POLICES OR ENDORSEMENTS, EITHER EXPRESSED OR IMPLIED,
OF AIR FORCE RESEARCH LABORATORY (AFRL/MLLN) OR THE U.S.
GOVERNMENT."**

1 9990610158

**MATERIALS AND MANUFACTURING DIRECTORATE
AIR FORCE RESEARCH LABORATORY
AIR FORCE MATERIEL COMMAND
WRIGHT-PATTERSON AFB, OH 45433-7817**


DTIC QUALITY INSPECTED 4

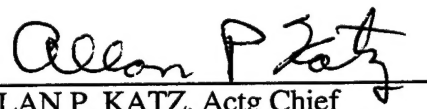
NOTICE

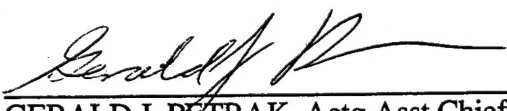
WHEN GOVERNMENT DRAWINGS, SPECIFICATIONS, OR OTHER DATA ARE USED FOR ANY PURPOSE OTHER THAN IN CONNECTION WITH A DEFINITELY GOVERNMENT-RELATED PROCUREMENT, THE UNITED STATES GOVERNMENT INCURS NO RESPONSIBILITY OR ANY OBLIGATION WHATSOEVER. THE FACT THAT THE GOVERNMENT MAY HAVE FORMULATED OR IN ANY WAY SUPPLIED THE SAID DRAWINGS, SPECIFICATIONS, OR OTHER DATA, IS NOT TO BE REGARDED BY IMPLICATION OR OTHERWISE IN ANY MANNER CONSTRUED, AS LICENSING THE HOLDER OR ANY OTHER PERSON OR CORPORATION, OR AS CONVEYING ANY RIGHTS OR PERMISSION TO MANUFACTURE, USE, OR SELL ANY PATENTED INVENTION THAT MAY IN ANY WAY BE RELATED THERETO.

THIS REPORT IS RELEASABLE TO THE NATIONAL TECHNICAL INFORMATION SERVICE (NTIS). AT NTIS, IT WILL BE AVAILABLE TO THE GENERAL PUBLIC, INCLUDING FOREIGN NATIONS.

THIS TECHNICAL REPORT HAS BEEN REVIEWED AND IS APPROVED FOR PUBLICATION.


THEODORE NICHOLAS
Ceramics Development & Materials
Behavior Branch
Metals, Ceramics & NDE Division


ALLAN P. KATZ, Actg Chief
Ceramics Development & Materials
Behavior Branch
Metals, Ceramics & NDE Division


GERALD J. PETRAK, Actg Asst Chief
Metals, Ceramics & NDE Division
Materials & Manufacturing Directorate

IF YOUR ADDRESS HAS CHANGED, IF YOU WISH TO BE REMOVED FROM OUR MAILING LIST, OR IF THE ADDRESSEE IS NO LONGER EMPLOYED BY YOUR ORGANIZATION, PLEASE NOTIFY, AFRL/MLLN, WRIGHT-PATTERSON AFB OH 45433-7817 TO HELP US MAINTAIN A CURRENT MAILING LIST.

COPIES OF THIS REPORT SHOULD NOT BE RETURNED UNLESS RETURN IS REQUIRED BY SECURITY CONSIDERATIONS, CONTRACTUAL OBLIGATIONS, OR NOTICE ON A SPECIFIC DOCUMENT.

REPORT DOCUMENTATION PAGE			Form Approved OMB No. 0704-0188	
<small>Public reporting burden for this collection of information is estimated to average 1 hour per response, including the time for reviewing instructions, searching existing data sources, gathering and maintaining the data needed, and completing and reviewing the collection of information. Send comments regarding this burden estimate or any other aspect of this collection of information, including suggestions for reducing this burden, to Washington Headquarters Services, Directorate for Information Operations and Reports, 1215 Jefferson Davis Highway, Suite 1204, Arlington, VA 22202-4302, and to the Office of Management and Budget, Paperwork Reduction Project (0704-0188), Washington, DC 20503.</small>				
1. AGENCY USE ONLY (Leave blank)		2. REPORT DATE OCTOBER 1997		3. REPORT TYPE AND DATES COVERED FINAL REPORT FOR JULY 1996 - OCTOBER 1997
4. TITLE AND SUBTITLE ON A MICROSTRUCTURAL THEORY OF PLASTIC DEFORMATION IN FACE-CENTERED-CUBIC MATERIALS			5. FUNDING NUMBERS C F33615-96-I-5264 PE 61102 PR 2302 TA B1 WU 07	
6. AUTHOR(S) RONALD L. BAGLEY--THE UNIVERSITY OF TEXAS AT SAN ANTONIO CALLIE C. BAST--THE UNIVERSITY OF TEXAS AT SAN ANTONIO DAVID L. CRANE--LOS ALAMOS, NEW MEXICO				
7. PERFORMING ORGANIZATION NAME(S) AND ADDRESS(ES) THE UNIVERSITY OF TEXAS AT SAN ANTONIO SAN ANTONIO, TX 78249			8. PERFORMING ORGANIZATION REPORT NUMBER	
9. SPONSORING/MONITORING AGENCY NAME(S) AND ADDRESS(ES) MATERIALS AND MANUFACTURING DIRECTORATE AIR FORCE RESEARCH LABORATORY AIR FORCE MATERIEL COMMAND WRIGHT-PATTERSON AFB, OH 45433-7750 POC: THEODORE NICHOLAS, AFRL/MLLN, 937-255-1347			10. SPONSORING/MONITORING AGENCY REPORT NUMBER AFRL-ML-WP-TR-1998-4105	
11. SUPPLEMENTARY NOTES				
12a. DISTRIBUTION AVAILABILITY STATEMENT APPROVED FOR PUBLIC RELEASE; DISTRIBUTION IS UNLIMITED			12b. DISTRIBUTION CODE	
13. ABSTRACT (Maximum 200 words) In this investigation, theoretical expression are developed for the threshold stress of plastic deformation and for the periodic spacing of deformation-induced dislocation microstructure in face-centered cubic materials. The process of plastic deformation in these materials, dislocation cross-slip, is modeled on the micro-scale (10-6m). This micro-scale mode is transformed into a macro-scale (structural component scale) engineering tool using the homogenization process, a form of volume averaging. The predicted flow stresses and periodic spacings compare very favorably with measured data.				
14. SUBJECT TERMS Plasticity, Virtual Work, Homogenization, Dislocations, Flow Stresses, Subgrain			15. NUMBER OF PAGES 61	
			16. PRICE CODE	
17. SECURITY CLASSIFICATION OF REPORT UNCLASSIFIED	18. SECURITY CLASSIFICATION OF THIS PAGE UNCLASSIFIED	19. SECURITY CLASSIFICATION OF ABSTRACT UNCLASSIFIED	20. LIMITATION OF ABSTRACT SAR	

TABLE OF CONTENTS

	Page
1. INTRODUCTION	1
2. THE PROCESS OF PLASTIC DEFORMATION	5
2.1 Observed Cross-Slip	5
2.2 Idealized Cross-Slip	8
3. HOMOGENIZATION	13
3.1 The Scales	13
3.2 Volume Averaging	14
4. THE CUBE'S STRAIN ENERGY DENSITY	18
4.1 The Shear Stress Distribution Across The Pile-Up	18
4.2 The Shape Function	25
4.3 The Assumed Elastic Displacement Fields	29
4.4 Elastic Strain Energy Density	30
5. THE VIRTUAL WORK FORMULATION	32
5.1 The Equilibrium Configuration in the Pile-up	33
5.2 The Work Densities	35
5.3 The Internal Heat Density	37
5.4 The Dislocation Energy Density	37
5.5 The Results of Virtual Work	39
6. RESULTS	42
7. DISCUSSION	51
8. REFERENCES	54

FIGURES

	Page
1 - Hierarchy of Scales	2
2 - A Slip-Plane with Barriers	6
3 - Channeling of Screw Components	7
4 - Slip-Induced Shear Stress Distribution	9
5 - The Cube	10
6 - Shear Stress Jumps in the Pile-Up	11
7 - A Comparison of the Two Shape Functions	28
8 - Measured Subgrain Diameter versus Theoretical Slip-Plane Spacing	44
9 - Measured Flow Stresses versus Theoretical Threshold for Aluminum	46
10 - Measured Flow Stresses versus Theoretical Threshold for OFHC Copper	47
11 - Measured Flow Stresses versus Theoretical Threshold for Nickel 200	48

TABLES

1 - Representative Values Of The Parameters	Page 26
2 - Material Parameters	49

ACKNOWLEDGMENTS

This research was sponsored by the Air Force Office of Scientific Research (Grant # F49620-97-1-0154), Wright Laboratory (Grant # F33615-96-1-5264), and the University of Texas at San Antonio. The authors are indebted to several of our colleagues for their willingness to review and comment on this research. In particular, the authors would like to thank Dr. David Davidson of Southwest Research Institute in San Antonio, Texas for his insight, encouragement and guidance. We are also indebted to Carla J. Bagley for preparing the drafts and the graphics.

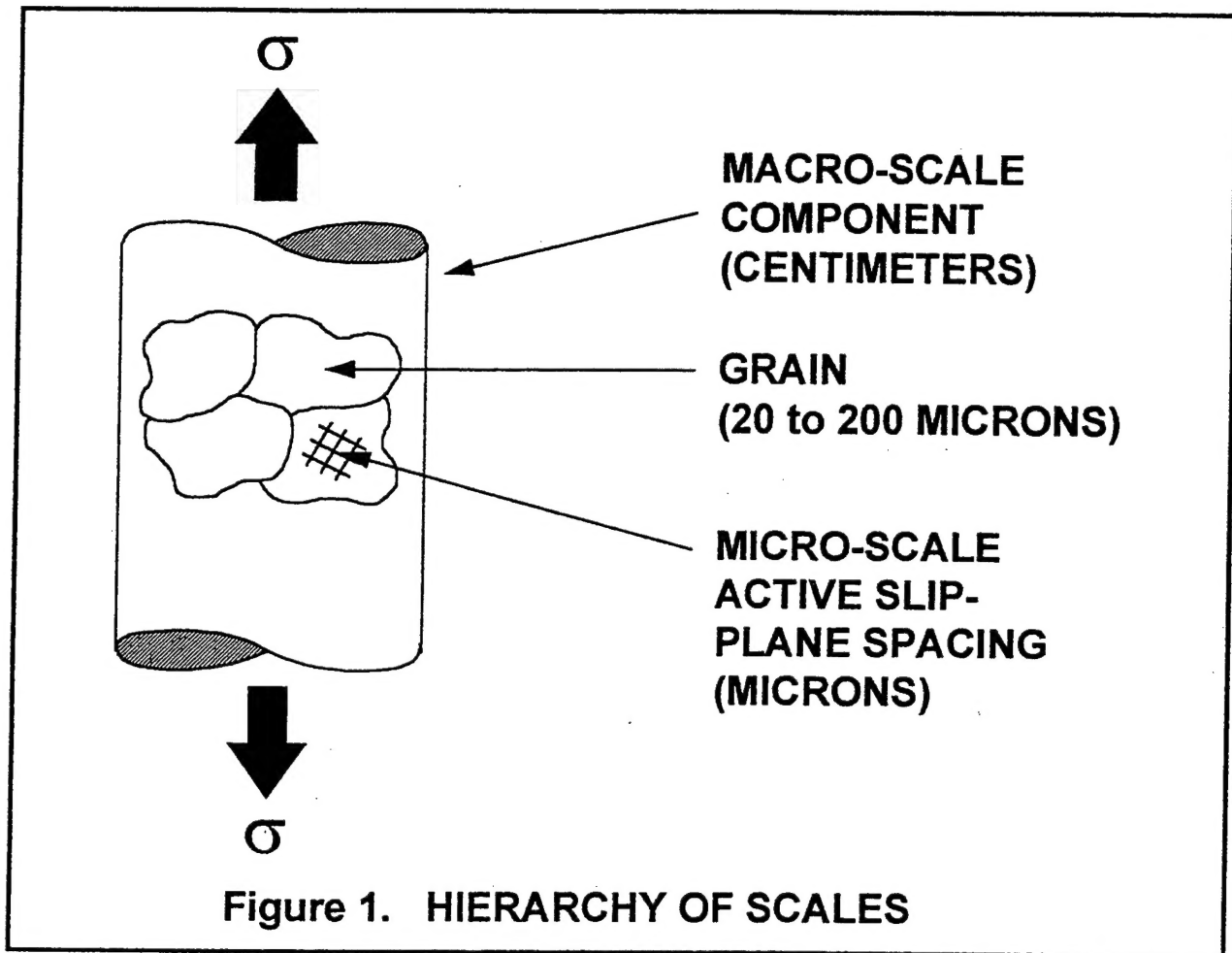
1. INTRODUCTION

The goal of this study is to establish approximate equilibrium relationships that govern a material's plastic deformation. The approach is to first model, on the micro-scale, the process that produces dislocations and plastic deformation and then bring the results to the macro-scale using the averaging process of homogenization (Christensen, 1979; Mura, 1987; Nemat-Nassar, 1993). The results are analytical expressions for the material's threshold flow stress and the spatial periodicity of its dislocation microstructure.

This study focuses on the fairly broad class of polycrystalline face-centered-cubic (FCC) metals. The dominant micro-mechanism of plastic deformation in these materials is dislocation slip. Experimental observations indicate that FCC materials develop a common mode of dislocation slip called cross-slip (Sestak, 1971). In these materials, cross-slip produces regularly spaced regions of densely packed dislocations where the spacing is observed to depend on the applied stress (Raj, 1996). This spacing in the material's dislocation microstructure is taken to be the characteristic length used in the homogenization process.

Homogenization formally relates the effects of the micro-scale heterogeneity in the microstructure to the material properties observed on the macro-scale, Figure 1. Specifically, the homogenization process incorporates the effects of localized elastic strain relief due to dislocation slip into the material's strain energy density. This density and the energy density for the extension of dislocations are folded into a virtual work formulation that produces the threshold flow stress and active slip-plane spacing relationships.

This study is based on the hypothesis that plastic deformation is a process that enables a loaded structural component to minimize its internal energy. Because the process of plastic



deformation is non-conservative, virtual work is employed rather than the principle of minimum potential energy used in the analysis of conservative elastic deformation.

There are a handful of articles in the literature applying variational techniques to the plastic deformation of solids (Gurtin, 1963; Hodge, 1962; Kachanov, 1959; Pian, 1957; Pian, 1958; Sanders, 1958). However, none of these applications attempt to describe the energies of dislocation extension and motion during plastic deformation. The principle of virtual work can be applied here as long as the non-conservative aspects of the process are adequately characterized.

A simplistic view is taken that the energy lost moving a dislocation, to be characterized through the introduction of a "friction stress," is the only non-conservative aspect of slip-generated plastic deformation. One might object to this approach because it does not account for the apparently non-conservative extension of dislocations during the process of plastic deformation. On the contrary, the extension of dislocations is viewed as the reversible (conservative) localization of strain energy in the distorted lattices surrounding their extended cores.

Treating dislocation extension as a reversible process is one of the cornerstones of this energy-based approach to plastic deformation. It is accepted that work done by the macro-scale external forces introduces elastic strain energy into the material. On the micro-scale, this strain energy partially manifests itself as shear stresses that perform work on internal slip-planes producing dislocation motion and extension. A fraction of the work done on the slip-planes is lost through the friction stress of dislocation motion, but the remaining fraction of this work

extends the length of dislocations. These processes are related quantitatively in the virtual work formulation.

The ability to employ energy methods that link deformation induced microstructure to parameters governing plastic deformation depends on the ability to model the process by which dislocation line length is extended to produce plastic deformation. This process is cross-slip.

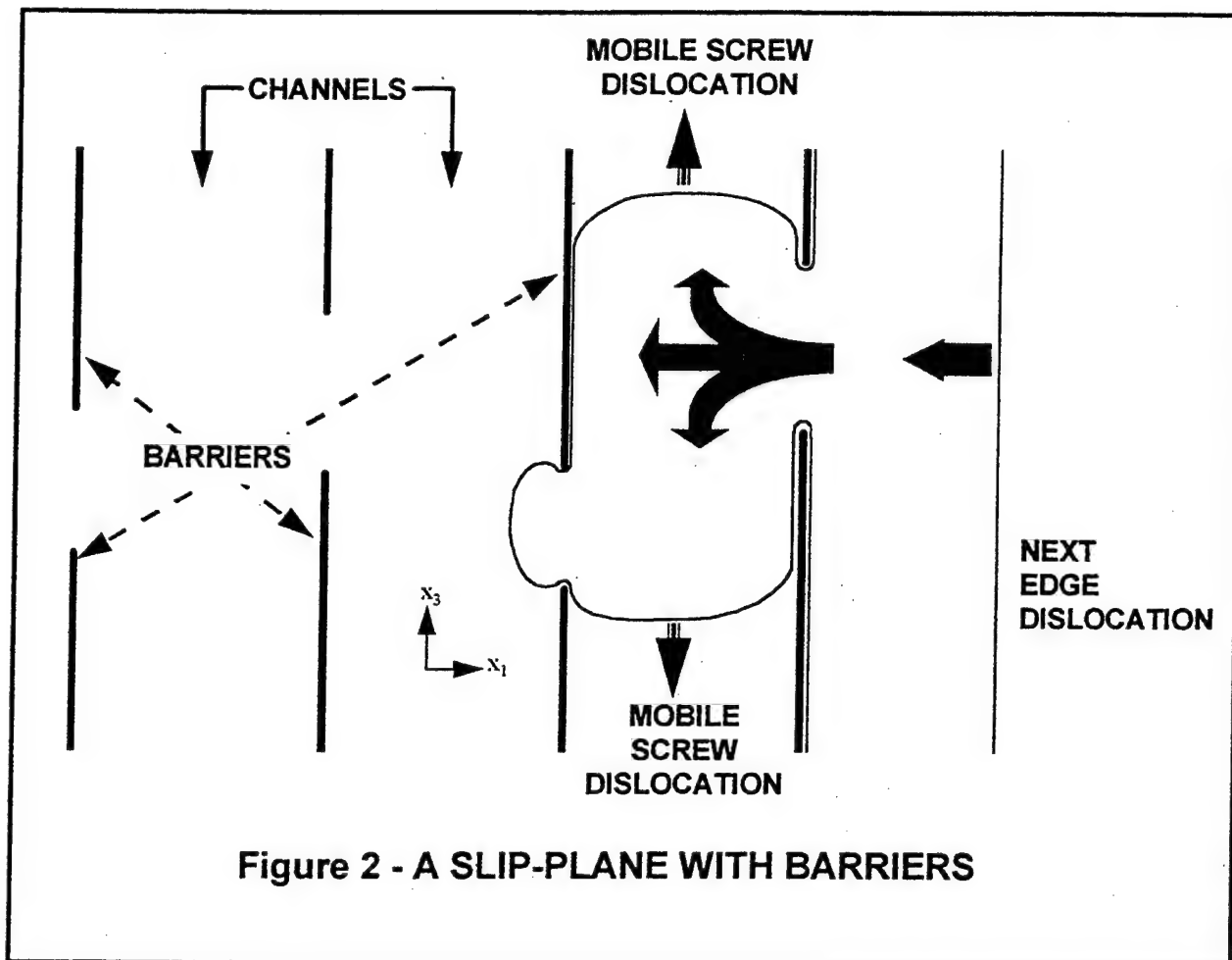
2. THE PROCESS OF PLASTIC DEFORMATION

2.1. Observed Cross-Slip

In this study, plastic deformation produced in an initially elastically distorted material is based on the notion that planes of atoms slide over one another through the motion of dislocations through the crystal lattice. Dislocations have two components: edge and screw dislocations. An edge dislocation is an extra half plane of atoms that terminates on and that is perpendicular to the plane along which it moves called the slip-plane. A screw dislocation is a hollow core surrounded by a helical pattern of atoms reminiscent of the thread on a screw. Screw dislocations, unlike edge dislocations, are capable of changing slip-planes during their motion. This process is called cross-slip.

Sestak and Seeger (Sestak, 1971) have pointed out that both FCC and BCC (body-centered cubic) metals exhibit cross-slip as the primary mechanism of plastic deformation in Stage III strain hardening. Stage I is the relatively uninhibited motion of dislocations called dislocation glide. Stage II strain hardening is the progressive formation of barriers that inhibit dislocation motion. Stage III is the cross-slipping of screw dislocations to get around these barriers, thus enabling dislocation motion, Figure 2. In polycrystalline materials, Stage III strain hardening and cross-slip start at plastic strain levels of at most a few percent. Hence, cross-slip is the primary mode of large plastic deformations in polycrystalline cubic materials.

Mughrabi's experimental observations (Mughrabi, 1987) are particularly valuable in characterizing the results of cross-slip. Mughrabi has observed the formation of the barriers depicted in Figures 2 and 3 for FCC materials. Furthermore, Mughrabi has observed that the barriers are made up of edge dislocations deposited by screw dislocations moving along the



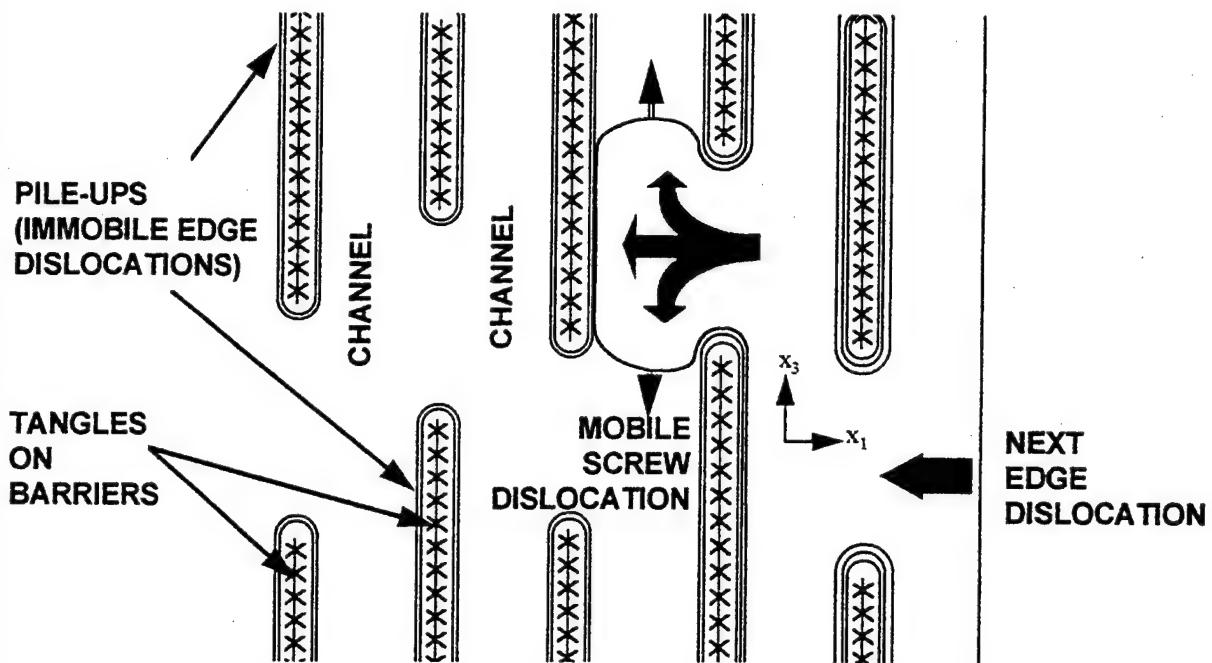


Figure 3. CHANNELING OF SCREW COMPONENTS

channels, shown schematically in Figures 2 and 3. In addition Mughrabi has measured the shear stress distribution that develops across dislocation pile-ups in the channels during plastic deformation, see Figures 4 and 6.

2.2 Idealized Cross-Slip

The model is based on Sestak's (Sestak, 1971) and Mughrabi's (Mughrabi, 1987) experimental observations. In particular, the model describes the motion of screw dislocations down channels formed by barriers. As each screw dislocation moves, it generates and deposits a dipole pair of edge dislocations on the surrounding barriers. When more screw dislocations move down the channel, more edge dislocations are extended and form pile-ups on the barriers. Eventually, the screw dislocations encounter obstacles and they cross-slip onto another slip-plane and circumvent these obstacles. The new extended edge components on the new slip-plane are now free to move. These edge components stop when they reach a barrier on the new slip-plane and the formation of new mobile screw components begins. As more barriers are formed, the screw dislocations are forced to move along progressively narrower channels.

As this process continues, a slip-plane segregates itself into three functionally distinct types of regions: the channels, the pile-ups, and the tangles, shown in Figure 3. The channels are the central gaps between the parallel pile-ups. The pile-ups are the edge dislocations pressed up against the tangles. The tangles are formed around the original barriers and are made up of edge dislocations forced to merge by the relatively high shear stress at the head of the pile-up shown in Figure 4.

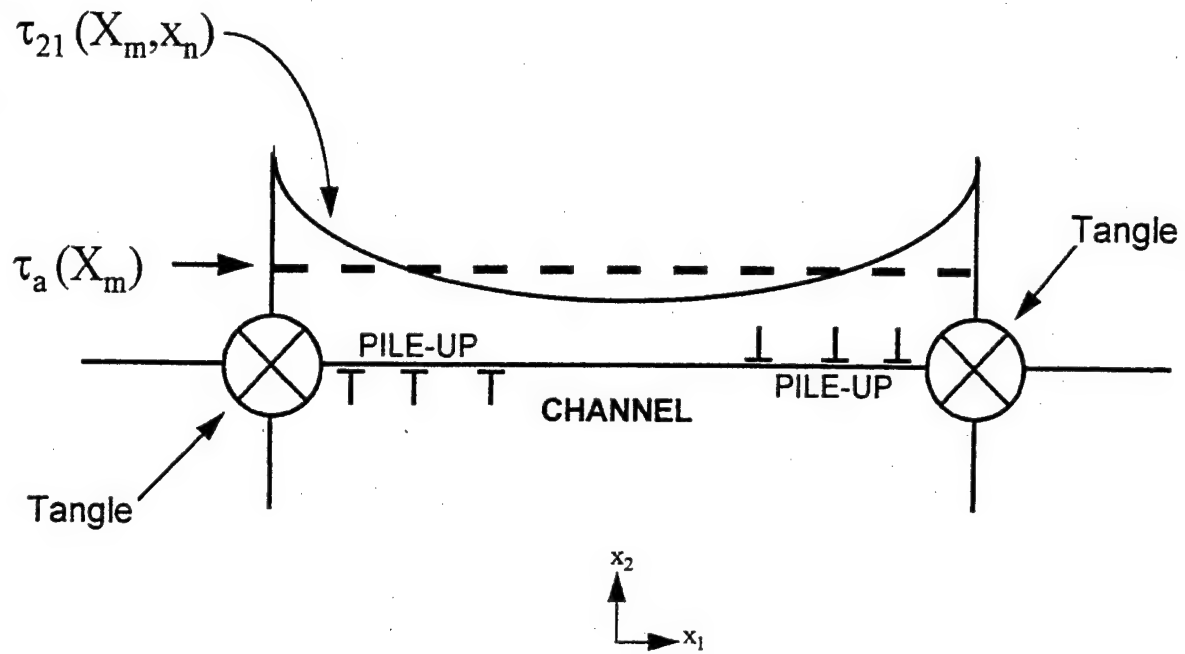
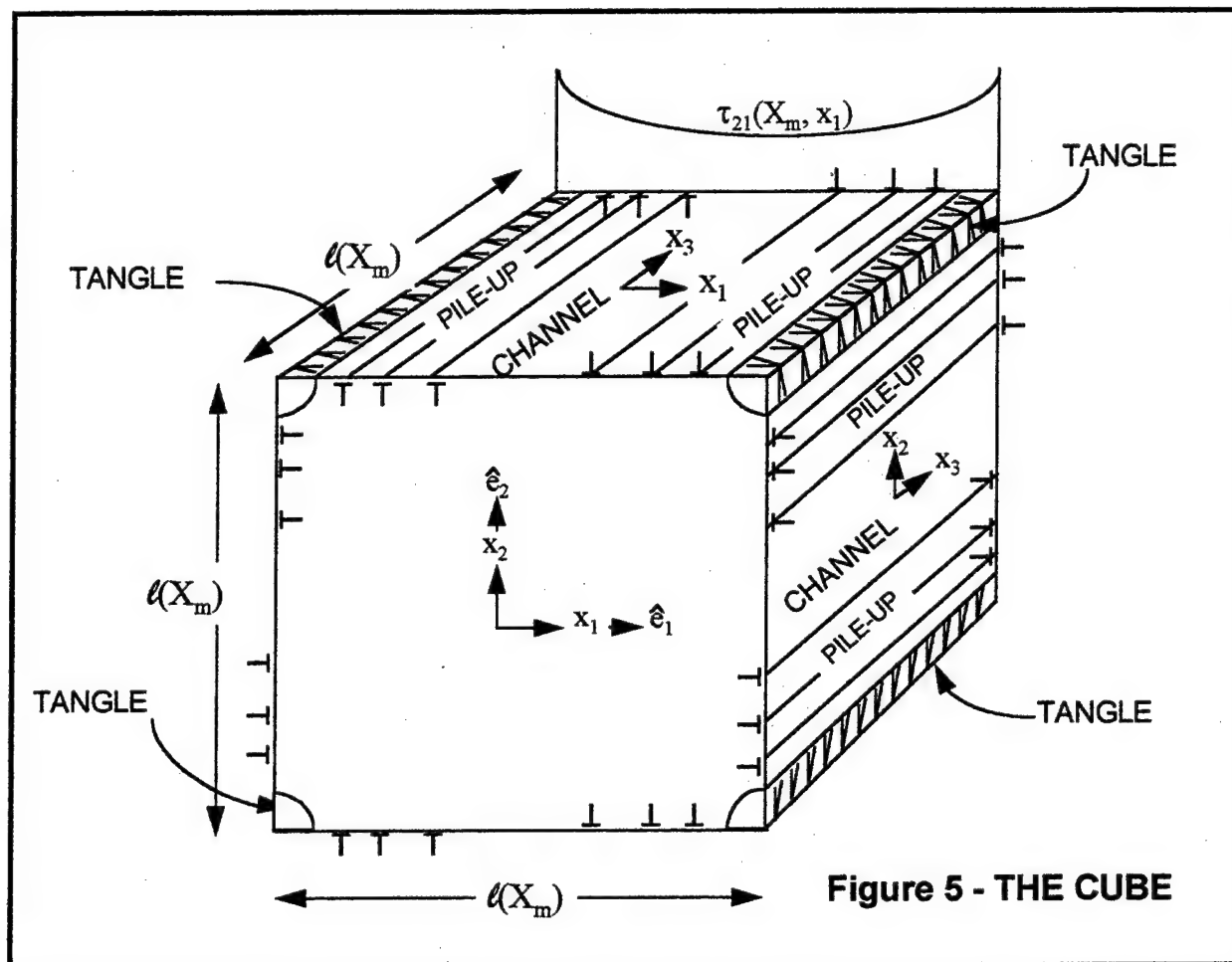


Figure 4 - SLIP-INDUCED SHEAR STRESS DISTRIBUTION



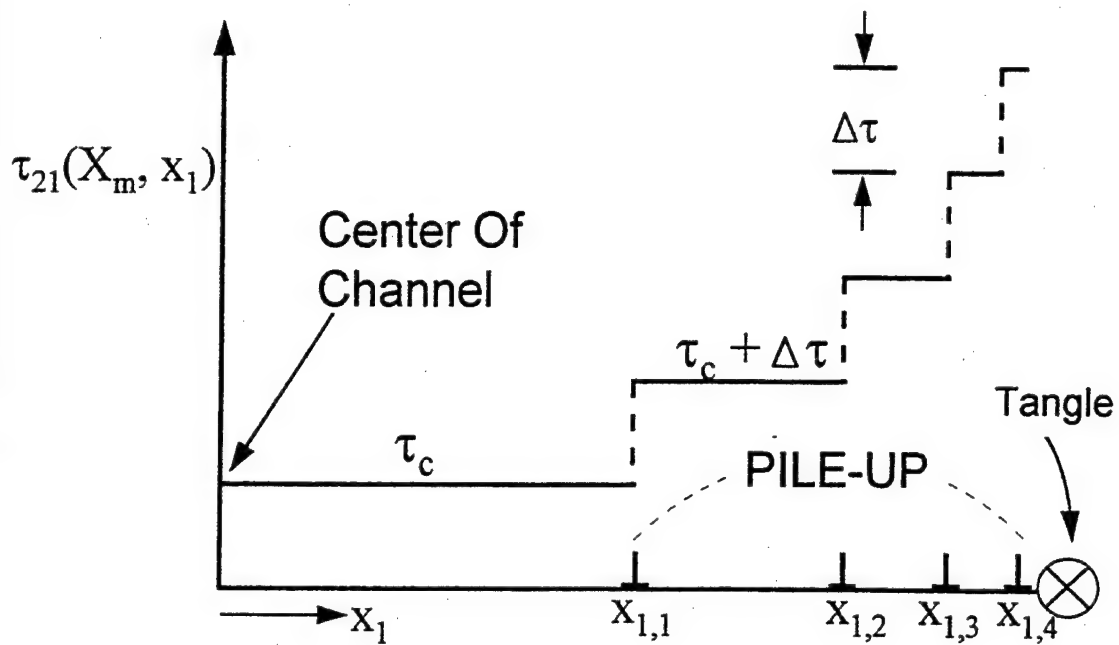


Figure 6 - SHEAR STRESS JUMPS IN THE PILE-UP

The shear stress varies across these three regions. In the channels, the shear stress decreases because the screw dislocations moving down the channels produce slip that relieves the local elastic shear strain. Local equilibrium redistributes the load onto the barriers (tangles) where there is no slip. The pile-ups are the transition regions from the low shear stress in the channels to the high shear stress in the tangles. In fact, Mughrabi has measured the shear stress variation across such a pile-up in copper (Mughrabi, 1987a).

As this pattern of channels, pile-ups and tangles continues to form, the dominant source of slip and plastic deformation is the screw dislocations moving along the channels. The cross-slip of the screw dislocations to circumvent any obstacles is the phenomenon that sustains this process.

3. HOMOGENIZATION

3.1 The Scales

To describe quantitatively the results of cross-slip, two sets of coordinates for two different scales are established: the macro-scale's global coordinates, X_m , and the micro-scale's local coordinates, x_n . The global coordinates are those traditionally used to perform structural analyses at the component level.

At any point in the material defined by the global coordinates, X_m , the local coordinates are defined by the local maximum shear stresses, $\tau_a(X_m)$. The directions of the first two local coordinates, $\hat{e}_1(X_n)$ and $\hat{e}_2(X_n)$, are the directions of the maximum shear stress, $\tau_a(X_n)$. The third local coordinate direction, $\hat{e}_3(X_n)$, is defined as a cross product of the first two and points in the direction of the intermediate valued principal normal stress. The domain for a local coordinate system is bounded by the active slip-planes assumed to be spaced $\ell(X_n)$ apart and aligned with the directions of $\tau_a(X_n)$, as shown in Figure 5.

The active slip-plane spacing, $\ell(X_m)$, is experimentally observed to be inversely dependent on the local average maximum shear stress $\tau_a(X_m)$. For values of $\tau_a(X_m)/G$ equal to 10^{-3} the slip-plane spacing is at most a few microns. (Raj, 1996a) Because this spacing is so small, it is assumed that the principal stresses, σ_i , and the unit vectors, \hat{e}_i , change very little between two adjacent parallel slip-planes. In other words, it is assumed that the global gradients of σ_i and \hat{e}_i times the slip-plane spacing $\ell(X_m)$ is small compared to their respective values of σ_i and one.

$$\Delta\sigma_i = \frac{\partial\sigma_i}{\partial X_m} \cdot \ell(X_m) \ll \sigma_i \quad (1)$$

$$|\Delta\hat{e}_i| = \left| \frac{\partial\hat{e}_i}{\partial X_m} \right| \cdot \ell(X_m) \ll 1 \quad (2)$$

These assumptions enable the local coordinates, x_n , to be taken as Cartesian within any cube having dimension $\ell(X_m)$, as shown in Figure 5. The four slip-planes, two parallel to \hat{e}_1 and \hat{e}_2 respectively, are taken to be four faces of the cube. The remaining two faces are assumed for convenience to have spacing $\ell(X_n)$ in the \hat{e}_3 direction. The origin of the local coordinate system is placed at the cube's center. All functions, that depend only on the global coordinates, X_m , are assumed to have a constant value within any cube. A primary reason for constructing the local coordinates and the cube is to define the volume over which the homogenization process is applied.

3.2 Volume Averaging

Homogenization is the formal process of volume averaging the effects of material heterogeneity at the micro-scale into a macro-scale formulation. In particular, the process averages the micro-scale effects of a composite material's fibers to produce an equivalent homogenous anisotropic material model on the macro-scale.

In this study, homogenization is used to incorporate the slip-induced micro-scale changes in the shear strain component of the strain energy density, while preserving the traditional elastic relationships between the average stresses on the macro-scale, $\bar{\sigma}_{ij}(X_m)$, and the average strains on the macro-scale, $\bar{\epsilon}_{ij}(X_m)$.

These average stresses and strains are defined by volume averaging and are called the equivalent homogenized stresses and strains.

$$\bar{\sigma}_{ij}(X_m) \equiv \frac{1}{V} \int_V \sigma_{ij}(X_m, x_n) dV \quad (3)$$

$$\bar{\epsilon}_{ij}(X_m) \equiv \frac{1}{V} \int_V \epsilon_{ij}(X_m, x_n) dV \quad (4)$$

Here the volume V is the cube and the integration is performed using the local coordinates, x_n .

Furthermore, the elastic displacement fields within any cube are defined in terms of the equivalent homogenized strains $\bar{\epsilon}_{ij}(X_m)$ and a locally varying displacement field $\tilde{u}_i(X_m, x_n)$.

$$u_i(X_m, x_n) \equiv \bar{\epsilon}_{ij}(X_m) \cdot x_j + \tilde{u}_i(X_m, x_n) \quad (5)$$

Here the locally varying components of displacement, \tilde{u}_i , are used to describe the local elastic distortion of the cube due to slip on the four slip-planes on its faces.

The resulting expression for the cube's strain fields is

$$\epsilon_{ij}(X_m, x_n) = \frac{1}{2} \left(\frac{\partial u_i}{\partial x_j} + \frac{\partial u_j}{\partial x_i} \right) = \bar{\epsilon}_{ij}(X_m) + \tilde{\epsilon}_{ij}(X_m, x_n) \quad (6)$$

Substituting this expression for the strains into equation 4, the definition of the equivalent homogenized strains, produces the following constraints on the locally varying strains,

$\tilde{\epsilon}_{ij}(X_m, x_n)$, and the displacement fields, $\tilde{u}_i(X_m, x_n)$.

$$\frac{1}{V} \int_V \tilde{\epsilon}_{ij}(X_m, x_n) dV = \frac{1}{V} \int_V \frac{1}{2} \left(\frac{\partial \tilde{u}_i}{\partial x_j} + \frac{\partial \tilde{u}_j}{\partial x_i} \right) dV = 0 \quad (7)$$

Hence, the cube's locally varying displacement fields must be constructed with these constraints in mind.

With these constraints satisfied, the resulting expression for the strain energy density in the cube is

$$\begin{aligned} U_e(X_m) &= \frac{1}{V} \int_V \frac{1}{2} \varepsilon_{ij}(X_m, x_n) E_{ijqp} \varepsilon_{qp}(X_m, x_n) dV \\ &= \frac{1}{2} \bar{\varepsilon}_{ij}(X_m) E_{ijqp} \bar{\varepsilon}_{qp}(X_m) + \Delta U_e(X_m) \end{aligned} \quad (8)$$

Note that the strain energy density has two components. The first is the strain energy associated with the cube's equivalent homogenized strains. The second is the change in the cube's strain energy density resulting from the local distortion of the cube due to slip.

As a direct consequence of the constraints given in equation 7, this second component is not a function of the equivalent homogenized strains, $\bar{\varepsilon}_{ij}(X_m)$. Hence the traditional energy relationship relating stress to strain is preserved

$$\frac{\partial U_e}{\partial \bar{\varepsilon}_{ij}} = E_{ijqp} \bar{\varepsilon}_{qp} = \bar{\sigma}_{ij} \quad (9)$$

for the equivalent homogenized stresses and strains.

Recall that the orientation of the cube is based on the directions of the local average maximum shear stresses, $\tau_a(X_m)$. Stated differently, the orientation of the cube at any point X_m is based on the directions of the maximum equivalent homogenized shear stresses. Also recall that the size of the cube is based on the spacing of the active slip-planes, $\ell(X_m)$. This spacing is experimentally observed to be stress dependent.

Consequently, the size and orientation of the cube are taken to be independent of the crystal lattice's orientation and anisotropy at the point X_m . For simplicity, the material is

assumed isotropic. Furthermore, all the distortions within the cube are taken to be linear and elastic: linear by choice and elastic because in this model, the plastic deformation is confined to the slip-planes on the boundaries of the cube.

4. THE CUBE'S STRAIN ENERGY DENSITY

The goal here is to construct the cube's strain energy density in the form of equation 8. The approach is to first construct approximate displacement functions in the form of equation 5.

$$u_i(X_m, x_n) \equiv \bar{\epsilon}_{ij}(X_m) \cdot x_j + \tilde{u}_i(X_m, x_n) \quad (5)$$

Here, the equivalent homogenized strains are assumed to be the known solutions of the macro-scale elasticity problem, posed in terms of the global coordinates, X_m . The locally varying, slip-generated displacement functions, $\tilde{u}_i(X_m, x_n)$, need be constructed to complete the expression for the cube's displacements, $u_i(X_m, x_n)$.

Approximations of the slip-generated displacements are based on the spatial dependence of the slip-generated shear stress and shear strain distributions across the pile-ups on the slip-planes, Figures 4 and 5. This spatial dependence is then used to construct shape functions that approximate the slip-generated elastic displacements in the cube, $\tilde{u}_i(X_m, x_n)$, and that satisfy the constraints in equation 7. The result is the displacement fields needed to construct the strain energy density for the cube, equation 5.

4.1 The Shear Stress Distribution Across The Pile-Up

The development begins with Eshelby's equation governing the equilibrium spacing of edge dislocations in a pile-up on the slip-plane. (Eshelby, 1951)

$$\sum_{\substack{i=1 \\ i \neq j}}^n \frac{\lambda}{x_{1,j} - x_{1,i}} + \tau_{21}(x_{1,j}) = 0 \quad j = 1, 2, 3, \dots, n \quad (10)$$

$$\lambda = \frac{Gb}{2\pi(1-\nu)} \quad (11)$$

Here G is the shear modulus, ν is Poisson's ratio, and b is the magnitude of the lattice's Burgers vector. Also $x_{1,j}$ is the micro-scale coordinate value of x_1 for the location of the j^{th} dislocation (shown in Figure 6), λ is the coefficient that describes the repulsive shear stress between two identical, parallel edge dislocations on the same slip-plane, and $\tau_{21}(x_{1,j})$ is the shear stress acting on the j^{th} dislocation.

Note that this slip-plane is defined by a constant value of the local coordinate of $x_2 = \ell(X_m)/2$. Because this coordinate value is constant, its presence is dropped from the notation for simplicity. In addition, the shear stress is taken to be independent of x_3 .

This development is further simplified by assuming that dislocations are only repelled through their nearest neighbors. This reduces equation 10 to

$$\begin{aligned} \frac{\lambda}{x_{1,j} - x_{1,j+1}} + \frac{\lambda}{x_{1,j} - x_{1,j-1}} + \tau_{21}(x_{1,j}) &= 0 & j = 2, 3, \dots, n \\ \frac{\lambda}{x_{1,2} - x_{1,1}} + \tau_{21}(x_{1,1}) &= 0 & j = 1 \end{aligned} \quad (12)$$

In equation 12, all terms in the summation in equation 10 are dropped except the $j + 1$ term and the $j - 1$ term which describe the interaction of the j^{th} dislocation with its nearest neighbors.

This nearest neighbor model accommodates Eshelby's observation that the local shear stress distribution increases one increment, $\Delta\tau$, as one passes each dislocation moving toward the head of the pile-up as portrayed in Figure 6. (Eshelby, 1951a)

$$\tau_{21}(x_{1,j}) = \tau_c + (j - 1) \Delta\tau \quad j = 1, 2, 3, \dots, n \quad (13)$$

Here τ_c is the shear stress in the center of the channel to the left of the dislocation at $x_{1,1}$, shown in Figure 6. The n^{th} dislocation in the pile-up is adjacent to the tangle.

Noting the recursive nature of equation 12, take the equation, starting with $j = 1$, and sequentially substitute it into the next higher indexed equation to replace the spacing terms. The result is an expression for the spacing between the j^{th} and $j+1^{\text{th}}$ dislocations

$$\frac{\lambda}{x_{1,j} - x_{1,j+1}} + \sum_{m=1}^j \tau_{21}(x_{1,m}) = 0 \quad (14)$$

The relationship indicates that this spacing is in fact affected by the stresses acting on all the j dislocations pressing on the $j+1^{\text{th}}$. However this cumulative stress effect is transmitted to the $j+1^{\text{th}}$ only through its nearest neighbor, the j^{th} dislocation. Using equation 13 to substitute for $\tau_{21}(x_{1,m})$ and performing the summation leads to

$$\frac{\lambda}{x_{1,j} - x_{1,j+1}} = - \left(j \cdot \tau_c + \frac{j(j-1) \Delta\tau}{2} \right) \quad (15)$$

Here, the first term describes the spacing between the j^{th} and the $j+1^{\text{th}}$ dislocations in the pile-up and the second term is the cumulative stress acting on all dislocations up to the j^{th} that produce this dislocation spacing.

This discrete algebraic relationship is approximated as a differential equation to derive a continuous function representing the spatial pattern of the dislocations and the resulting shear stress and shear strain distributions on the slip-plane. To this end, first replace the index j with the discrete valued function, $n(x_{1,j+1})$. This function is the number of dislocations in the pile-up between the center of the channel, $x_1 = 0$, and the location of the $j+1^{\text{th}}$ dislocation, $x_1 = x_{1,j+1}$, shown in Figure 6. Next, replace $n(x_{1,j+1})$ with its continuous representation, $n(x_1)$, expressed as a function of the local coordinate x_1 .

$$j \rightarrow n(x_{1,j+1}) \rightarrow n(x_1) \quad (16)$$

Now, observe that the inverse dislocation spacing $(x_{1,j} - x_{1,j+1})^{-1}$ may be viewed as the approximate spatial gradient of $n(x_{1,j+1})$ or equivalently the spatial derivative of $n(x_1)$,

$$(x_{1,j} - x_{1,j+1})^{-1} \cong -\frac{dn(x_1)}{dx_1} \quad (17)$$

when $x_{1,j+1}$ is replaced by the local continuous variable x_1 . Substituting these changes into equation 15 leads to the following non-linear differential equation for $n(x_1)$.

$$-\lambda \frac{dn(x_1)}{dx_1} + \left(n(x_1)\tau_c + \frac{n(x_1)(n(x_1) - 1)}{2} \Delta\tau \right) = 0 \quad (18)$$

Using partial fractions, equation 18 can be rewritten as

$$\frac{dn(x_1)}{n(x_1)} - \frac{dn(x_1)}{n(x_1) + 2\beta - 1} = \frac{(2\beta - 1)\Delta\tau}{2\lambda} dx_1 \quad (19)$$

where $\beta = \tau_c / \Delta\tau$. Integrating equation 19 yields

$$n(X_m, x_1) = \frac{N(X_m)(2\beta - 1) \exp \left[a \left(x_1 - \frac{\ell(X_m)}{2} \right) \right]}{(2\beta - 1) + N(X_m) \left(1 - \exp \left[a \left(x_1 - \frac{\ell(X_m)}{2} \right) \right] \right)} \quad (20)$$

where $a = \frac{(2\beta - 1)\Delta\tau}{2\lambda}$. (21)

Here $n(X_m, x_1)$ satisfies the boundary condition

$$n \left(X_m, \frac{\ell(X_m)}{2} \right) = N(X_m) \quad (22)$$

where $N(X_m)$ is the total number of dislocations in the pile-up. The important result here is equation 20, the spatial distribution of dislocations in the pile-up expressed as a function of the local coordinate x_1 .

This spatial distribution leads to the expression for the shear stress as it varies across the pile-up. The continuous analogue of equation 13 expressed here

$$\tau_{21}(X_m, x_1) = \tau_c + n(X_m, x_1) \cdot \Delta\tau \quad (23)$$

produces the expression for the shear stress on the slip-plane.

$$\tau_{21}(X_m, x_1) = \tau_c + n(X_m, x_1) \Delta\tau = \tau_c + \frac{N(X_m)(2\beta-1) \exp\left[a\left(x_1 - \frac{\ell(X_m)}{2}\right)\right] \Delta\tau}{(2\beta-1) + N(X_m)\left(1 - \exp\left[a\left(x_1 - \frac{\ell(X_m)}{2}\right)\right]\right)} \quad (24)$$

To complete this expression for the shear stress, two issues need to be resolved. The first is whether or not β (the ratio of τ_c to $\Delta\tau$) is a function of the total number of dislocations in the pile-up, $N(X_m)$. The second is to express τ_c and $\Delta\tau$ in terms of $\tau_a(X_m)$, the equivalent homogenized shear stress on the slip-plane.

The first issue is addressed by observing that the shear stress expression, equation 24, has a characteristic exponential length, a^{-1} . This characteristic length is used to estimate the increment of slip-induced shear strain relief produced in the channel. Recall that as each screw dislocation moves down a channel, Figure 3, the material above the dislocation's path moves the magnitude of one Burgers vector, b , relative to the material under the dislocation's path. Assume that half of this relative motion, $b/2$, contributes to strain relief above the slip-plane

and that the other half contributes to strain relief below the slip-plane. Hence, the increment of shear strain relief is estimated to be half the slip distance b divided by the characteristic length, a^{-1} .

The shear strain drop in the channel due to the passage of a screw dislocation is

$$\Delta\gamma = \frac{b}{2} \cdot \frac{1}{a^{-1}} \quad (25)$$

This increment of shear strain drop in the channel produces the increment of shear stress drop across the newly formed edge dislocation deposited on the pile-up by the passing screw dislocation, Figure 6. From equations 11 and 21, see that

$$\Delta\tau = \frac{G b}{2} a = \frac{(2\beta - 1) \Delta\tau \pi (1 - \nu)}{2} \quad (26)$$

and $\Delta\tau$ divides out of this relationship leaving β as a constant.

$$\beta = \frac{1}{2} + \frac{1}{\pi (1 - \nu)} \quad \tau_c = \beta \Delta\tau \quad (27)$$

The choice of a^{-1} as the normalizing length for the increment of elastic strain relief is somewhat arbitrary.

Using energy arguments, Eshelby determined that the shear stresses in a pile-up are multiples of τ_c . (Honeycombe, 1984) Taking β , the ratio $\tau_c/\Delta\tau$ to be one and subsequently replacing $\Delta\tau$ in equation 13 with τ_c produces a quantitative expression of Eshelby's conclusion.

$$\tau_{21}(x_{1,j}) = \tau_c + (j-1)\tau_c \quad j = 1, 2, 3, \dots, n \quad (28)$$

Note that the expression for β , equation 27, yields values very close to one.

The remaining issue is to determine the relationship between the shear stress in the channel, τ_c , and the equivalent homogenized maximum shear stress, $\tau_a(X_m)$. To develop this relationship, the definition of equivalent homogenized stress, equation 3, is used.

$$\bar{\sigma}_{ij}(X_m) \equiv \frac{1}{V} \int_V \sigma_{ij}(X_m, x_n) dV \quad (3)$$

Throughout this study, this relationship is enforced by insisting that the stress, acting on any plane within the cube that is parallel to a face and integrated over the area of the plane, be equal to the corresponding equivalent homogenized stress multiplied by the area of the plane. Stated mathematically this condition is

$$\bar{\sigma}_{ij}(X_m) \cdot A_i = \int_{A_i} \sigma_{ij}(X_m, x_n) dA_i \quad (29)$$

Note that multiplying this relationship by the cube's dimension, $\ell(X_m)$, and dividing by the cube's volume produces equation 3, the definition of equivalent homogenized stress.

Applying equation 29 to the shear stress distribution on the slip-plane takes the form

$$\tau_a(X_m) \cdot \ell^2(X_m) = \int_{-\ell(X_m)/2}^{\ell(X_m)/2} \int_{-\ell(X_m)/2}^{\ell(X_m)/2} \tau_{21}(X_m, x_1) dx_1 dx_3 \quad (30)$$

Substituting the expression for the shear stress, equation 24, into this equation and evaluating the integrals results in

$$\tau_a(X_m) \equiv \tau_c + \frac{4\lambda}{\ell(X_m)} \ln \left(\frac{N(X_m)}{2\beta-1} + 1 \right) \quad (31)$$

subject to the condition that

$$\tau_c \cdot \ell(X_m) \gg 2\lambda \quad (32)$$

Representative values (Shankaranarayan, 1995) of these parameters are given in Table 1 and for these values equation 32 holds.

Solving for the shear stress in the channel, τ_c , in terms of the equivalent homogenized maximum shear stress, $\tau_a(X_m)$, produces

$$\tau_c(X_m) = \tau_a(X_m) - \frac{4\lambda}{\ell(X_m)} \ln \left(\frac{N(X_m)}{2\beta-1} + 1 \right) \quad (33)$$

and the shear stress jump at each dislocation in the pile-up is

$$\Delta\tau(X_m) = \frac{\tau_c(X_m)}{\beta} \quad (34)$$

At this point, the expression for the approximate shear stress distribution on the slip-plane, equation 24, is complete.

4.2 The Shape Function

Based on equation 24, the shear stress distribution on the slip-plane can be expressed as

$$\tau_{21}(X_m, x_1) = \tau_c(X_m) + n(X_m, x_1) \cdot \Delta\tau(X_m) \quad (35)$$

where $n(X_m, x_1)$ is defined in equation 20. Dividing this expression by $2G$ produces the shear strain distribution on the slip-plane.

$$\varepsilon_{21}(X_m, x_1) = \frac{\tau_c(X_m)}{2G} + n(X_m, x_1) \cdot \frac{\Delta\tau(X_m)}{2G} \quad (36)$$

Note that the function $n(X_m, x_1)$ describes the local (micro-scale) variation in the strain.

Consequently, $n(X_m, x_1)$ would be an excellent candidate function to approximate the slip-induced elastic distortion in the cube, except for one major drawback. The square of this

TABLE 1. REPRESENTATIVE VALUES OF THE PARAMETERS

$$G = 42 \text{ GPa.}$$

$$N(X_m) = 15$$

$$b = 2.56 * 10^{-10} \text{m.}$$

$$\ell(X_m) = 10^{-6} \text{ m.}$$

$$\nu = 0.33$$

$$\Delta\tau = \tau_c = 30 \text{ MPa.}$$

$$\beta = 1$$

function has no known closed-form expression for its integral. This integral is needed to sum the strain energy over the cube. As a result, $n(X_m, x_1)$ will be approximated by a simple exponential function $\phi(X_m, x_1) \cdot N(X_m)$.

$$\phi(X_m, x_1) \equiv \exp \left[B \left(\frac{2\sqrt{x_1^2}}{\ell(X_m)} - 1 \right) \right] \quad (37)$$

Here the parameter B is chosen to satisfy the homogenization constraint expressed in equation 30.

The resulting approximation of the shear stress distribution on the slip-plane is

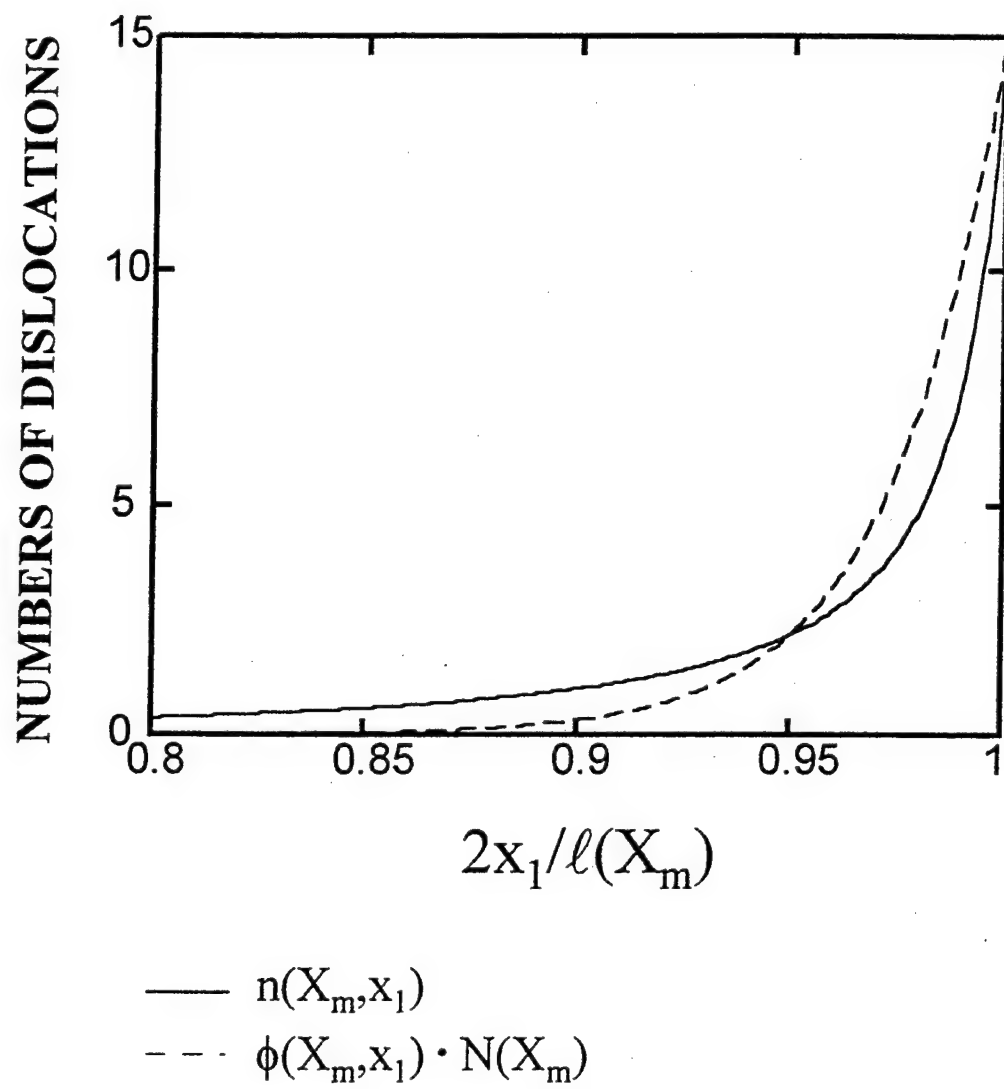
$$\tau_{21}(X_m, x_1) = \tau_c(X_m) + \phi(X_m, x_1) \cdot N(X_m) \cdot \Delta\tau(X_m) \quad (38)$$

Substituting this expression into equation 30 and choosing B such that equation 31 is satisfied produces the following expression for B.

$$B = \frac{N(X_m)\Delta\tau(X_m)}{\frac{4\lambda}{\ell(X_m)} \ln \left[\frac{N(X_m)}{2\beta-1} + 1 \right]} \quad (39)$$

In effect, $\phi(X_m, x_1) \cdot N(X_m)$ is an exponential function of x_1 that replaces $n(X_m, x_1)$, a ratio of exponential functions of x_1 , and that produces the same equivalent homogenized shear stress when integrated over the slip-plane. A comparison of these two functions is shown in Figure 7, for $N(X_m) = 15$. The agreement between these functions steadily improves as $N(X_m)$ decreases in value to one.

FIGURE 7. A COMPARISON OF THE TWO SHAPE FUNCTIONS



For simplicity of notation $\phi(X_m, x_1)$ will be expressed as $\phi(x_1)$.

$$\phi(x_1) \equiv \exp \left[B \left(\frac{2\sqrt{x_1^2}}{\ell(X_m)} - 1 \right) \right] \quad (40)$$

The square of this function has a known expression for its integral and $\phi(x_1)$ will be used to approximate the elastic distortion of the cube due to slip on its bounding slip-planes.

Before proceeding, it is important to note that $\phi(x_1)$, evaluated at $x_1 = 0$, is much less than one, or else $\tau_{21}(X_m, 0)$ will not be approximately equal to $\tau_c(X_m)$ in the center of the channel (equation 38). Using the representative values in Table 1, B has a value of 8 and $\phi(0) = \exp[-B]$ is very small compared to one.

4.3 The Assumed Elastic Displacement Fields

The following assumed displacement functions are constructed in the form prescribed by equation 5 and in compliance with the homogenization requirements expressed in equations 3 & 4.

$$\begin{aligned} u_1(X_m, x_1, x_2) &= \bar{\epsilon}_{11}(X_m) x_1 + \bar{\epsilon}_{12}(X_m) x_2 + \frac{\lambda}{G} \ln \left[\frac{N(X_m)}{2\beta - 1} + 1 \right] \phi(x_1) \int_0^{x_2} \phi(\eta) d\eta \\ &\quad + \frac{N(X_m) \Delta \tau(X_m)}{2G(B-1)} \int_0^{x_2} (1 - \phi(\eta)) d\eta (1 - \phi(x_1)) - \frac{x_2}{2G} \cdot \frac{4\lambda}{\ell(X_m)} \ln \left[\frac{N(X_m)}{2\beta - 1} + 1 \right] \\ u_2(X_m, x_1, x_2) &= \bar{\epsilon}_{22}(X_m) x_2 + \bar{\epsilon}_{21}(X_m) x_1 + \frac{\lambda}{G} \ln \left[\frac{N(X_m)}{2\beta - 1} + 1 \right] \int_0^{x_1} \phi(\xi) d\xi \phi(x_2) \\ &\quad + \frac{N(X_m) \Delta \tau(X_m)}{2G(B-1)} (1 - \phi(x_2)) \int_0^{x_1} (1 - \phi(\xi)) d\xi - \frac{x_1}{2G} \cdot \frac{4\lambda}{\ell(X_m)} \ln \left[\frac{N(X_m)}{2\beta - 1} + 1 \right] \\ u_3(X_m, x_3) &= \bar{\epsilon}_{33}(X_m) x_3 \end{aligned} \quad (41)$$

The equivalent homogenized strains appear explicitly in the displacement functions. Recall that the local coordinate directions were chosen such that $\bar{\epsilon}_{31}(X_m), \bar{\epsilon}_{13}(X_m), \bar{\epsilon}_{32}(X_m)$ and $\bar{\epsilon}_{23}(X_m)$ are zero. The terms in $u_1(X_m, x_1, x_2)$ and $u_2(X_m, x_1, x_2)$ not containing the homogenized strains are chosen such that the shear stresses on the 1 and 2 faces of the cube match the shear stress distribution, equation 38, on the slip-planes. In addition, these terms are chosen such that the equivalent homogenized stress and strain relationships, equations 3 and 4, are satisfied throughout the cube.

The method used to construct these displacement functions is based on the observation that $\phi(x)$ is an even function of x , and its integral and derivative are odd functions of x . The displacements are constructed such that the slip-induced shear strains (shear stresses) are even functions on their respective planes. When this is the case, the slip-induced extensional strains (normal stresses) are odd functions on their respective planes. Hence, the slip-induced normal stresses integrate to zero on their respective planes and the slip-induced shear stresses integrate to zero when the channel shear stress, $\tau_c(X_m)$, is adjusted using equation 33. When the slip-induced stresses integrate to zero over their respective planes, the integrals of the total stresses over their respective planes yield the equivalent homogenized stresses, equation 3.

4.4 Elastic Strain Energy Density

The cube's strains are determined from the displacement fields, equation 41, and are then substituted into equation 8

$$\varepsilon_{ij}(X_m, x_n) = \frac{1}{2} \left[\frac{\partial u_i(X_m, x_n)}{\partial x_j} + \frac{\partial u_j(X_m, x_n)}{\partial x_i} \right] \quad (8)$$

to determine the cube's strain energy density.

$$U_e = \frac{1}{V} \int_V \frac{1}{2} \varepsilon_{ij}(X_m, x_n) E_{ijqp} \varepsilon_{qp}(X_m, x_n) dV \quad (42)$$

The resulting expression for the density is

$$U_e = \frac{1}{2} \bar{\varepsilon}_{ij}(X_m) E_{ijqp} \bar{\varepsilon}_{qp}(X_m) - \frac{N^2(X_m) \Delta \tau^2(X_m)}{12G} \cdot \frac{(1-\nu)}{(1-2\nu)} \cdot \frac{(B^3 - 3B^2 + 6)}{B^2 (B-1)^2} \quad (43)$$

where

$$\bar{\varepsilon}_{ij}(X_m) = \begin{bmatrix} \bar{\varepsilon}_{11}(X_m) & \bar{\varepsilon}_{12}(X_m) & 0 \\ \bar{\varepsilon}_{21}(X_m) & \bar{\varepsilon}_{22}(X_m) & 0 \\ 0 & 0 & \bar{\varepsilon}_{33}(X_m) \end{bmatrix} \quad (44)$$

As expected, the strain energy density has two components: the first expressed in terms of the equivalent homogenized strains; and the second is the strain energy released by the cube due to slip. Note that the anticipated elastic relationship between the homogenized stresses and strains, equation 9, follows directly from equation 43.

5. THE VIRTUAL WORK FORMULATION

The equilibrium relationships governing the slip-induced plastic deformation are determined using the principle of virtual work. Here, the principle of virtual work is employed such that at equilibrium, the virtual work, δW , equals the virtual increase in the materials internal energy, δU .

$$\delta W = \delta U \quad (45)$$

Here W and U are respectively the work done and internal energy per unit mass of the material. It is assumed that the elastic and thermal strains are sufficiently small to make the material's mass density essentially constant. Under these circumstances, energy per unit mass and energy per unit volume differ only by a constant scaling factor of mass density. Hence, energy per unit mass is replaced by energy per unit volume throughout this study.

The internal energy is taken to have three components.

$$U = Q + U_e + U_d \quad (46)$$

Q is the specific internal energy based on the temperature of the cube. U_e is the strain energy density for the elastic distortion within the cube. U_d is the strain energy density for the lattice distortions surrounding the dislocations in the pile-ups and tangles on the surface of the cube.

The specific work, W , is taken to have two components.

$$W = W_e + W_s \quad (47)$$

W_e is the work per unit volume performed through virtual elastic displacements. W_s is the work per unit volume performed through virtual slip displacements.

Substituting equations 46 and 47 into equation 45 yields the variational relationship that produces the equilibrium relationships.

$$\delta W_e + \delta W_s = \delta Q + \delta U_e + \delta U_d \quad (48)$$

Here, it is assumed that at equilibrium, there is no heat flux across the surfaces of the cube.

Thus, δQ arises only through dissipative work done on the surfaces of the cube.

To this point, only one of the five terms in equation 48 (the cube's strain energy density, U_e) has been constructed. Three of the four remaining terms will be constructed based on the notion of an equilibrium configuration in the pile-ups.

5.1 The Equilibrium Configuration in the Pile-up

To facilitate the development of the remaining work and energy expressions, it is valuable to first address the concept of an "equilibrium" configuration for the dislocation pile-ups on the slip-planes. "Equilibrium" first occurs when the number of edge dislocations in the pile-up, $N(X_m)$, becomes sufficiently large to force the edge dislocation in the pile-up nearest the tangle to merge into the tangle. At the onset of equilibrium, the shear stress at the head of the pile-up is just below the critical value needed to force the leading dislocation into the tangle. As each new edge dislocation, generated in the channel and deposited in the pile-up, raises the shear stress at the head of the pile-up to this critical value, the leading dislocation merges into the tangle. After this merging has taken place, the shear stress at the head of the pile-up drops back just below the critical value. The result is that for every edge dislocation that moves into the pile-up, there is another edge dislocation forced out of the pile-up and into the tangle keeping $N(X_m)$ constant. When $N(X_m)$ reaches this steady value, the pile-up is said to be in "equilibrium."

As this process continues, the net number of dislocations in the pile-up, $N(X_m)$, remains unchanged, while each edge dislocation in the pile-up moves, in sequence, closer to the head of the pile-up and eventually merges into the tangle. The number of edge dislocations forced to merge into the tangles during equilibrium is labeled $S(X_m)$.

Davidson has observed that edge dislocations imbed themselves in tangles when forced within a distance of approximately four Burgers vectors, $4b$ (Davidson, 1997). Using equation 15 to determine the number of dislocations in a pile-up required to produce this spacing yields

$$-\frac{\lambda}{4b} = -\left(j \tau_c(X_m) + \frac{j(j-1) \Delta\tau(X_m)}{2}\right) \quad (49)$$

Replacing j with $N(X_m)$ produces the expression for the spacing at the head of a pile-up.

$$N(X_m) \tau_c(X_m) + \frac{N(X_m)(N(X_m)-1) \Delta\tau(X_m)}{2} = \frac{\lambda}{4b} \quad (50)$$

Recall that

$$\lambda = \frac{Gb}{2\pi(1-\nu)} \quad (11)$$

Taking β to be one simplifies solving the quadratic expression, equation 50, for $N(X_m)$.

$$N(X_m) \cong \frac{1}{2} \left(\frac{2\lambda}{b\Delta\tau(X_m)} \right)^{1/2} \quad (51)$$

Using the appropriate data given in Table 1, the resulting value of $N(X_m)$ is 13.

5.2 The Work Densities

There are two sources of virtual work performed on the cube: the work done through elastic displacements, δW_e , and the work done through virtual slip displacements, δW_s . The work done through virtual elastic displacements is that work done by the component's surface tractions elastically distorting the body. Applying the divergence theorem to the global elasticity problem, it can be shown that the work density of the surface tractions can be expressed in terms of the equivalent homogenized stresses and strains. (Fung, 1965)

$$\delta W_e = \bar{\sigma}_{ij}(X_m) \delta \bar{\epsilon}_{ij}(X_m) \quad (52)$$

However, the surface tractions also perform work that permanently changes the shape of the body through slip displacements on the internal slip-planes. Because the cube's shear stress distribution and the pattern of slip on its slip-plane are known, the expression for the work density due to slip can be constructed directly on the micro-scale.

$$2W_s = \frac{4}{V} \int_{A_2} \int_{s_1(X_m, x_1)}^{s_2(X_m, x_1)} \tau_{21}(X_m, x_1) \cdot b \cdot ds(X_m, x_1) dA_2 \quad (53)$$

The integral term is equivalent to the work done on the four faces of the cube that are slip-planes. Because the cube shares each of these four faces with one of four other cubes, the work done on the four slip-planes is twice the work done on the cube. $b \cdot ds(X_m, x_1)$ is the differential of the relative slip motion through which the shear stress performs work.

If it is assumed that the pile-up is in an "equilibrium" state, as previously discussed, the work integral over the slip-plane can be straightforwardly evaluated. During equilibrium, a screw dislocation moving down the channel deposits an edge dislocation on each pile-up and one

dislocation moves out of each pile-up and into a tangle. During this process, the screw dislocation causes slip of one Burgers vector in the channel. In addition, each edge dislocation in the pile-up advances one position toward the tangle as the closest edge dislocation merges into the tangle. This produces slip of one Burgers vector throughout the pile-up. The result is that there is a slip of one Burgers vector over channel and the two pile-ups. Hence, the differential slip $ds(X_m, x_1)$ is independent of x_1 during equilibrium. Furthermore, the amount of slip that occurs during equilibrium is the number of dislocations pushed from the head of the pile-up into the tangle, $S(X_m)$.

With these observations, one can reduce the work density integral to

$$W_s = \frac{2bS(X_m)}{V} \int_{A_2} \tau_{21}(X_m, x_1) dA_2 \quad (54)$$

Recall that any locally varying stress, like $\tau_{21}(X_m, x_1)$, integrates over the area on which it acts to the area times the equivalent homogenized stress, equation 30. Hence the expression for the work density for slip becomes

$$W_s = \frac{2bS(X_m) \tau_a(X_m) \ell^2(X_m)}{\ell^3(X_m)} = \frac{2\tau_a(X_m) S(X_m)b}{\ell(X_m)} \quad (55)$$

Identifying $S(X_m) \cdot b/\ell(X_m)$ as the plastic shear strain, the variation of the work density due to slip is seen to be

$$\delta W_s = 2\tau_a(X_m) \delta \left(\frac{S(X_m)b}{\ell(X_m)} \right) \quad (56)$$

5.3 The Internal Heat Density

The internal heat density of the cube is raised by the energy dissipated by the friction stress, τ_f , that resists the motion of a dislocation across the slip-plane. Using the arguments presented in the previous section and the observation that the friction stress is uniform over the slip-planes produces the following expression for the change in the cube's internal heat density.

$$2\Delta Q = \frac{4}{V} \int_{A_2} \tau_f \cdot S(X_m) \cdot b \, dA_2 \quad (57)$$

Upon evaluation, this integral reduces to

$$\Delta Q = \frac{2\tau_f S(X_m)b}{\ell(X_m)} \quad (58)$$

Again, identifying the plastic shear strain as $S(X_m) \cdot b/\ell(X_m)$, the variation of Q is seen to be

$$\delta Q = 2\tau_f \delta \left(\frac{S(X_m)b}{\ell(X_m)} \right) \quad (59)$$

It should be pointed out that the uniform slip on the slip-plane is produced by screw dislocations moving down the channel and edge dislocations advancing toward the head of the pile-up. Edge and screw dislocations have slightly different friction stresses. The friction stress used here, τ_f , should be viewed as an average friction stress.

5.4 The Dislocation Energy Density

All dislocations deposited in the pile-ups on the slip-plane occur in dipole pairs (opposite types on the same plane). As a screw dislocation moves down the channel, the two deposited edge dislocations (one onto each pile-up) are each of the opposite type. This deposited dipole

pair forces the lead dislocation in each pile-up into their respective tangle. The two dislocations forced into the tangles are also a dipole pair.

During equilibrium, the increase in the dislocation energy on a slip-plane is the number of dipole pairs forced into their tangles, $S(X_m)$, times the energy of each pair. The energy of each pair has two parts: the strain energies of the pair plus the energy required to push each dislocation up against its nearest neighbor.

$$2U_d = \frac{4S(X_m) \cdot \ell(X_m)}{\ell^3(X_m)} \left[\frac{Gb^2}{2\pi(1-\nu)} \ln \left(1 + \frac{\ell(X_m)}{b} \right) + \frac{2Gb^2}{2\pi(1-\nu)} \ln \left(1 + \frac{\ell(X_m)}{4b} \right) \right] \quad (60)$$

The first term in the brackets is the energy per unit dislocation length for a dipole-pair separated a distance, $\ell(X_m)$. (McClintock, 1966) The second term is the energy per unit dislocation length required to push the dipole pair against their respective nearest neighbors a distance of $4b$ away. Recall that $4b$ was the critical dislocation spacing at the head of the pile-up at equilibrium.

Note that as the distance separating the elements of the dipole pair, $\ell(X_m)$, tends to zero, the energy of the dislocation dipole pair tends to zero as well. In other words, if the dipole pair were to recombine in the absence of the friction stress, all its energy would be fully released. Consequently, this expression for the strain energy around the dipole pairs indicates that the energy is recoverable, hence conservative.

The dislocation energy density can be accurately approximated by

$$U_d = \frac{Gb^2 S(X_m)}{\pi(1-\nu) \ell^2(X_m)} \ln \left(\frac{\ell^3(X_m)}{16b^3} \right) \quad \frac{\ell(X_m)}{b} \gg 1 \quad (61)$$

5.5 The Results of Virtual Work

Having expressions for all the components of the virtual work formulation, the representative values of the parameters in Table 1 can be used to check the relative values of the energy densities. This process reveals that the change in the cube's elastic strain energy density due to slip is roughly comparable to the dislocation energy density for plastic strains, $S(X_m) \cdot b/\ell(X_m)$, of one percent. For much larger plastic strains, the dislocation energy density is much larger than the slip-induced change in the cube's strain energy density. The slip-induced strains apparently remove strain energy from the interior of the cube and transfer the energy to the regions near the four tangles. Hence, the slip-induced change in the cube's strain energy density is relatively small for plastic strains over five percent and it is dropped from consideration.

Substituting equations 52, 56, 59, 61 and 43 (without the term for the strain energy drop due to slip) into equation 48 yields

$$\begin{aligned} \bar{\sigma}_{ij}(X_m) \delta \bar{\epsilon}_{ij}(X_m) + 2\tau_a(X_m) \delta \left(\frac{S(X_m)b}{\ell(X_m)} \right) = \\ 2\tau_f \delta \left(\frac{S(X_m)b}{\ell(X_m)} \right) + E_{ijqp} \bar{\epsilon}_{qp}(X_m) \delta \bar{\epsilon}_{ij}(X_m) + \delta \left(\frac{Gb^2 S(X_m)}{\pi(1-\nu)\ell^2(X_m)} \ln \left(\frac{\ell^3(X_m)}{16b^3} \right) \right) \end{aligned} \quad (62)$$

The plastic shear strain, $S(X_m) \cdot b/\ell(X_m)$, contains two parameters that are free to vary: the number of dislocations pushed from a pile-up into a tangle, $S(X_m)$, and the edge length of the cube, $\ell(X_m)$.

Letting these two parameters vary independently, along with the elastic strains $\bar{\epsilon}_{ij}(X_m)$, produces the following results.

$$\begin{aligned}
& \left[\bar{\sigma}_{ij}(X_m) - E_{ijqp} \bar{\epsilon}_{qp}(X_m) \right] \delta \bar{\epsilon}_{ij}(X_m) \\
& + \left[2\tau_a(X_m) - 2\tau_f - \frac{Gb}{\pi(1-\nu)\ell(X_m)} \ln \left(\frac{\ell^3(X_m)}{16b^3} \right) \right] \cdot \frac{b \delta S(X_m)}{\ell(X_m)} \\
& + \left[-2\tau_a(X_m) + 2\tau_f + \frac{Gb \cdot 2}{\pi(1-\nu)\ell(X_m)} \ln \left(\frac{\ell^3(X_m)}{16b^3} \right) - \frac{3Gb}{\pi(1-\nu)\ell(X_m)} \right] \frac{S(X_m)b}{\ell^2(X_m)} \delta \ell(X_m) = 0
\end{aligned} \tag{63}$$

Setting the coefficient of the variation of the elastic strains to zero yields the traditional linear elastic constitutive law posed in terms of the equivalent homogenized stresses and strains.

$$\bar{\sigma}_{ij}(X_m) = E_{ijqp} \bar{\epsilon}_{qp}(X_m) \tag{64}$$

Setting the coefficient of the variation $\delta S(X_m)$ to zero yields an expression for the threshold flow stress of the material.

$$\tau_a(X_m) = \tau_f + \frac{Gb}{2\pi(1-\nu)\ell(X_m)} \ln \left(\frac{\ell^3(X_m)}{16b^3} \right) = \tau_{th}(X_m) \tag{65}$$

Close examination of the energies (from which this expression follows) indicates that this is the threshold value of $\tau_a(X_m)$ for which sufficient work is performed on the slip-plane to extend the edge dislocations through the motion of the screw dislocations down the channels. When $\tau_a(X_m)$ drops below this critical value, dislocation motion and extension stops and plastic deformation due to cross-slip ceases. Note that the expression for the threshold flow stress, $\tau_{th}(X_m)$, depends on the slip-plane spacing, $\ell(X_m)$.

Setting the coefficient of $\delta\ell(X_m)$ in equation 63 to zero produces an expression for the equilibrium spacing of the active slip-planes.

$$\tau_a(X_m) = \tau_f + \frac{Gb}{\pi(1-\nu)\ell(X_m)} \left(\ln \left(\frac{\ell^3(X_m)}{16b^3} \right) - \frac{3}{2} \right) \quad (66)$$

Given the maximum equivalent homogenized shear stress, $\tau_a(X_m)$, the only remaining unknown in this equation is the slip-plane spacing.

In summary, the virtual work has produced both the elastic and plastic equilibrium conditions for the material. The elastic equilibrium conditions are the traditional stress-strain relationships from which the maximum equivalent homogenized shear stress follows, $\tau_a(X_m) = \bar{\sigma}_{21}(X_m)$. Using $\tau_a(X_m)$ and equation 66, the equilibrium slip-plane spacing, $\ell(X_m)$, is determined. Using $\ell(X_m)$ and equation 65, the threshold flow stress, $\tau_{th}(X_m)$, is determined. Using $\tau_a(X_m)$ and $\ell(X_m)$ in equations 33, 34 and 51 produces the values for the equilibrium number of dislocations in a pile-up $N(X_m)$, the channel stress $\tau_c(X_m)$, and the shear stress jump $\Delta\tau(X_m)$. Introducing these results into equations 24 and 41 produces the shear stress distribution on the slip-planes and the elastic displacement fields for the cube. Hence, the equilibrium problem for plastic response is solved.

Note that the plastic equilibrium conditions, equations 65 and 66, appear in the form of stress-strain relationships when the dimensionless ratio, $b/\ell(X_m)$, is interpreted as an increment of plastic shear strain. Both equations relate an increment of plastic shear strain to a shear stress using the shear modulus and Poisson's ratio.

6. RESULTS

The virtual work formulation has produced theoretical expressions for the equilibrium spacing of the active slip-planes, $\ell(X_m)$, and the threshold flow stress, $\tau_{th}(X_m)$. The applied stress $\tau_a(X_m)$ determines the equilibrium active slip-plane spacing. The actual slip-plane spacing determines the threshold flow stress.

In this study, the slip-plane spacing, $\ell(X_m)$, is advanced as the parameter that governs the formation of an FCC material's heterogeneous subgrain microstructure. In particular, the active slip-plane spacing is taken to be the diameter of subgrains that are observed to form during plastic deformation in FCC materials. A subgrain is a region of relatively few dislocations surrounded by a shell of highly concentrated dislocations. It is hypothesized that the cube (bounded by four slip-planes containing dislocation pile-ups and tangles) is a representative model of the subgrain.

If this hypothesis holds, considerable data in the literature can be used to test the theoretical expressions for the active slip-plane spacing and the threshold flow stress. Specifically, Raj, et al, have collected data on subgrain diameter versus applied stress for many materials including aluminum and copper. Based on this data, Raj has constructed an empirical relationship between applied stress and subgrain diameter (Raj, 1996b). In addition, Varma along with three of his students have measured flow stresses and the corresponding subgrain diameters in three FCC metals: aluminum (Sil, 1993), copper (Shankaranarayan, 1995), and nickel (Rao, 1993).

These measured data will be used to test both theoretical relationships. First, Raj's curve fit for subgrain diameter versus applied stress will be compared to the theoretical expression for

active slip-plane spacing versus applied stress, equation 66. Second, subgrain diameter will be used in place of active slip-plane spacing in the theoretical expression for the threshold flow stress, equation 65. The resulting predicted threshold flow stresses will be compared with Varma's measured flow stresses.

Raj's expression relating applied stress to subgrain diameter is posed in terms of a uniaxial tensile stress, σ ; the subgrain diameter, d_s ; and an empirical parameter K chosen to produce the best curve-fit for the measured data. The relationship is

$$\frac{d_s}{b} = K \left(\frac{G}{\sigma} \right)^m \quad (67)$$

where $K = 23$ and $m = 1.0$. Converting the tensile stress to the shear stress on the active slip-planes, $\tau_a(X_m) = \sigma/2$, produces

$$\frac{d_s}{b} = 11.5 \left(\frac{G}{\tau_a(X_m)} \right) \quad (68)$$

Plotting this experimentally based empirical relationship, Figure 8, against the theoretical relationship, equation 66, demonstrates the excellent agreement. The friction stress, τ_f in equation 66, in FCC metals is relatively small compared to the applied stress and is taken to be zero in this comparison. The shear stress/shear modulus ratio varies from creep response loading (10^{-5}) up to yield strengths (10^{-3}) and finally up to flow stress (10^{-2}). The excellent agreement seen here is advanced as strong evidence supporting the hypothesis that the active slip-plane spacing is the progenitor of the observed heterogeneous distribution of dislocations in the subgrain microstructures of FCC materials.

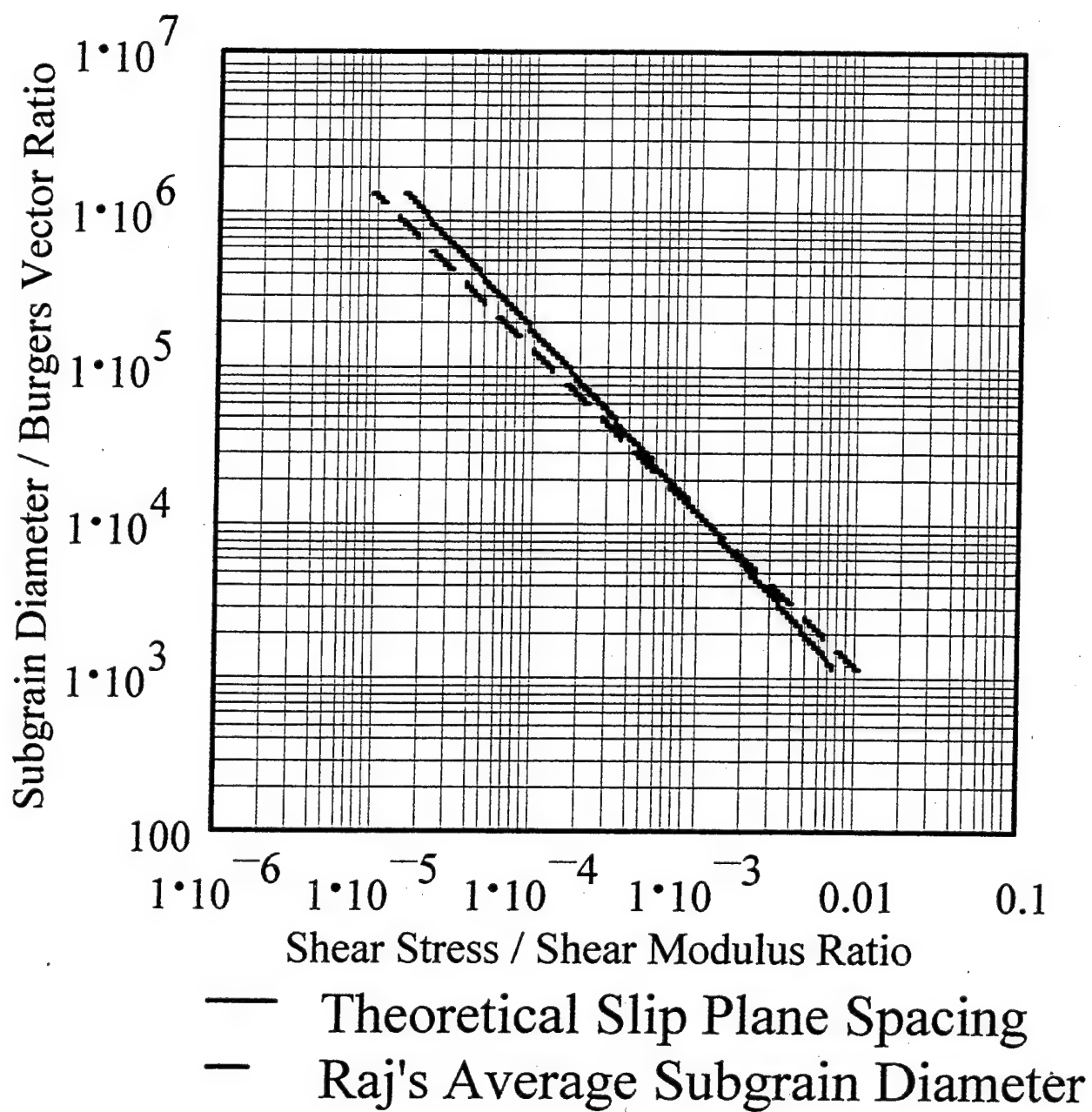


FIGURE 8. MEASURED SUBGRAIN DIAMETER VERSUS THEORETICAL SLIP-PLANE SPACING

Using this hypothesis, one can predict a threshold flow stress when subgrain diameter is used in place of active slip-plane spacing, equation 65 . A summary of the results are shown in Figure 9 for aluminum, Figure 10 for copper, and Figure 11 for nickel. The values of the material parameters used to predict the threshold flow stress are given in Table 2. Each material's reported Peierls stress (Honeycombe, 1984a) is used for its friction stress, τ_f .

In Figures 9, 10 and 11, the measured flow stresses have been adjusted. Varma and his students reported the measured flow stresses as nominal tensile stresses. The constant volume assumption for large plastic deformation in thin tensile specimens of original length, L_0 , and cross sectional area, A_0 ,

$$V_0 = A_0 L_0 = A(L_0 + \Delta L) \quad (69)$$

has been employed here to estimate true tensile stress from nominal tensile stress. This relationship enables one to estimate the reduced cross sectional area, A ,

$$A = A_0 \left(1 + \frac{\Delta L}{L}\right)^{-1} = A_0 (1 + \epsilon_p)^{-1} \quad (70)$$

based on Varma's measured plastic tensile strain, ϵ_p . Subsequently, the true tensile flow stress is estimated from the measured nominal flow stress, based on the level of plastic strain.

$$\sigma = \sigma_0 (1 + \epsilon_p) \quad (71)$$

All of the flow stresses shown in Figures 9, 10 and 11 are the estimated true stresses based on Varma's measured nominal flow stresses and measured plastic strains.

The theoretical tensile threshold flow stresses shown in Figures 9, 10 and 11 are twice the theoretical shear threshold flow stresses predicted using equation 65. For the most part, the theoretical thresholds are right where they should be. For copper and nickel the thresholds are

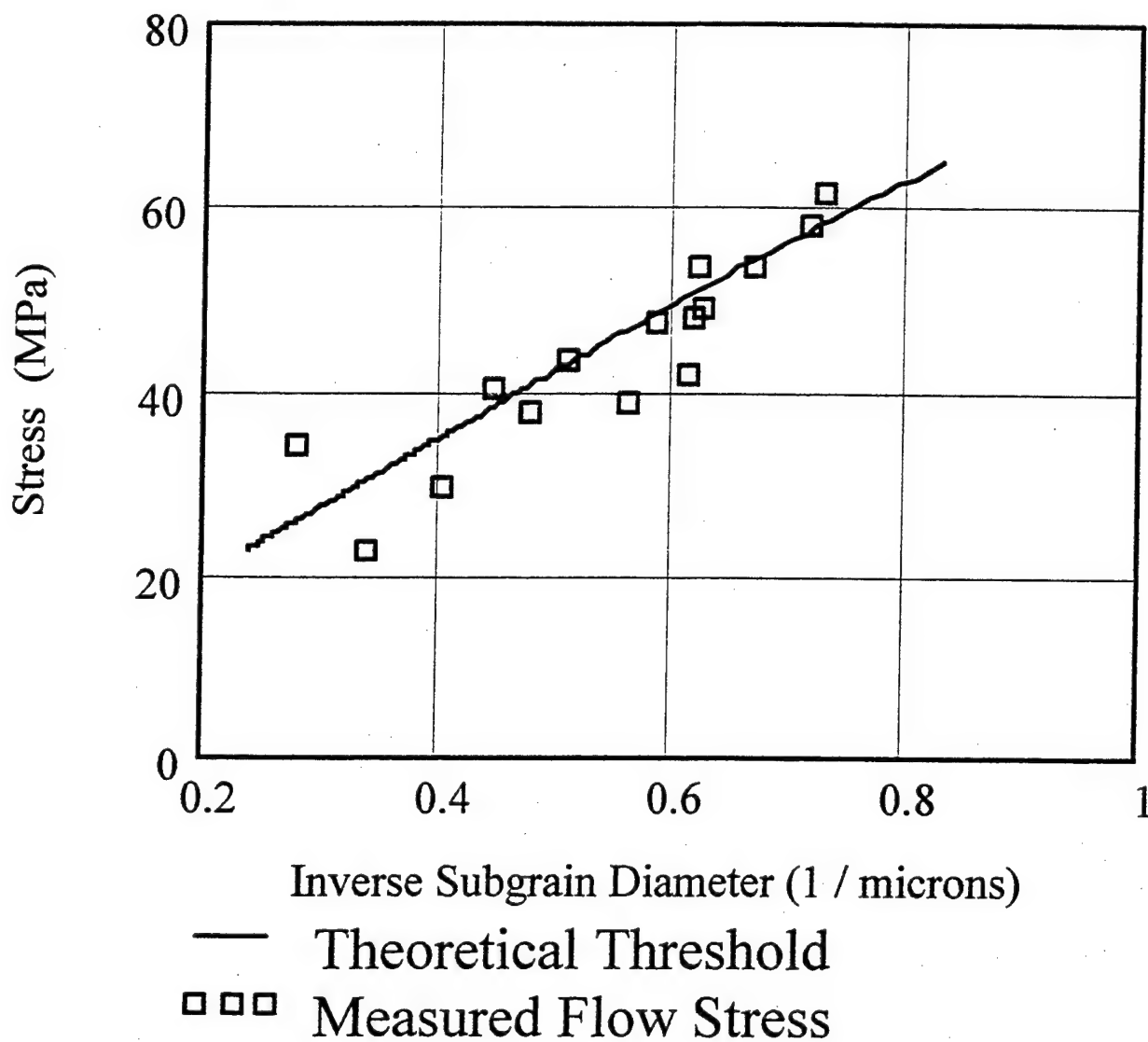


FIGURE 9. MEASURED FLOW STRESSES VERSUS
THEORETICAL THRESHOLD FOR ALUMINUM

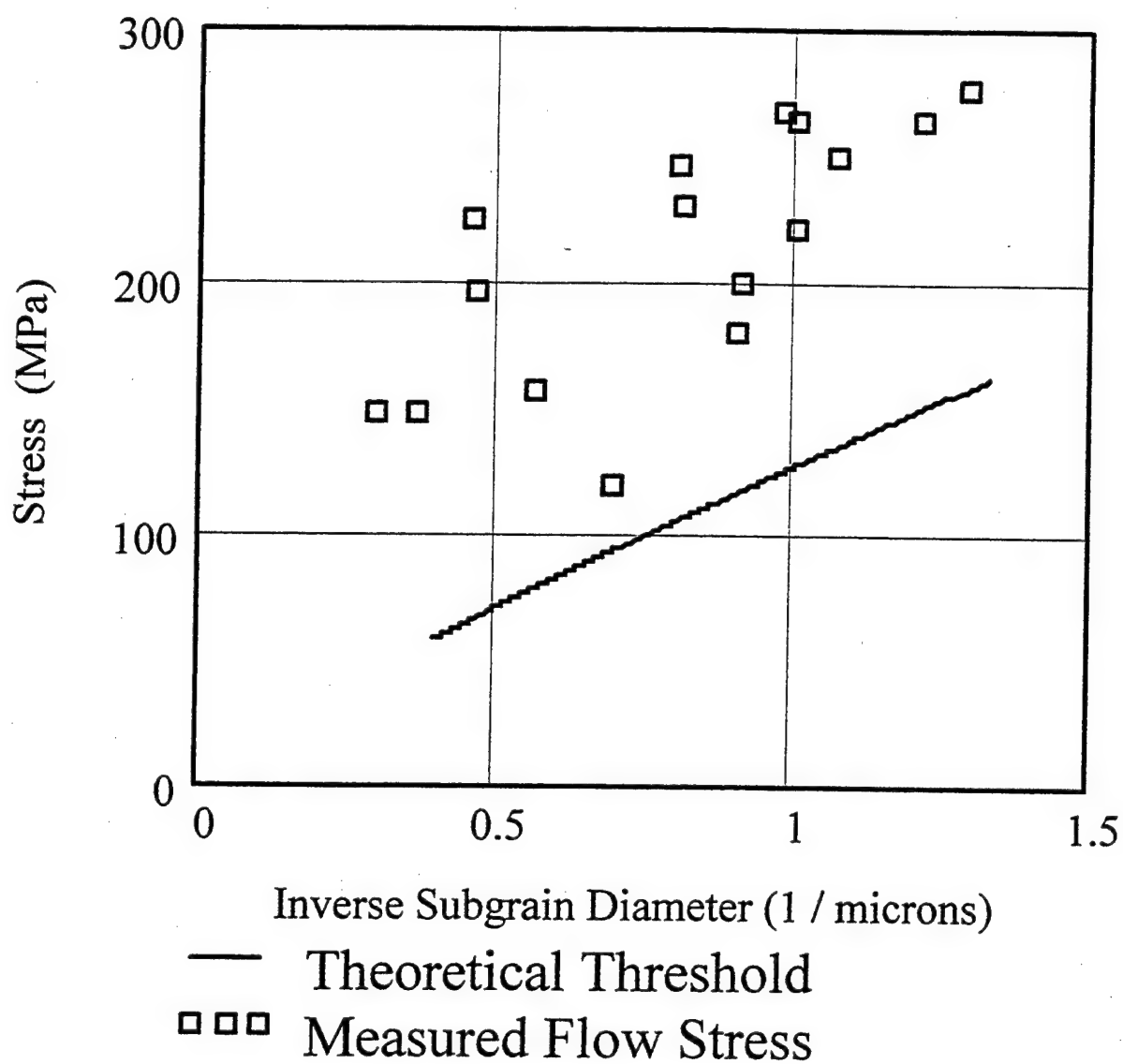


FIGURE 10. MEASURED FLOW STRESSES VERSUS THEORETICAL THRESHOLD FOR OFHC COPPER

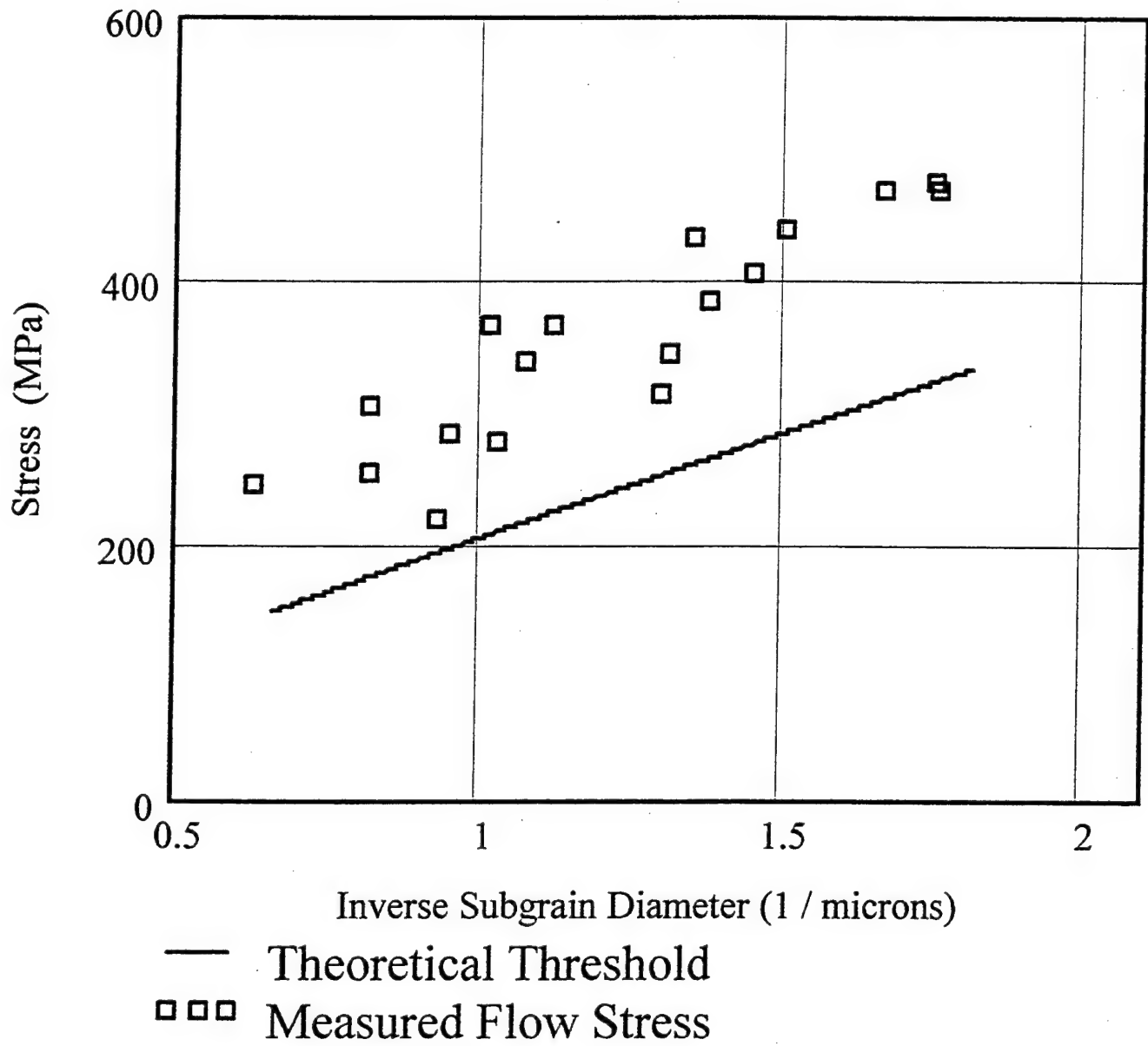


FIGURE 11. MEASURED FLOW STRESSES VERSUS
THEORETICAL THRESHOLD FOR NICKEL 200

TABLE 2. MATERIAL PARAMETERS

	G	ν	b	τ_f
Aluminum	25 GPa	0.33	0.286 nm	1.0 MPa
Copper	46 GPa	0.34	0.256 nm	1.0 MPa
Nickel	76 GPa	0.31	0.250 nm	5.0 MPa

below the adjusted measured flow stresses. For aluminum, the theoretical threshold is higher than it should be. Recall that the threshold stress is the stress below which all plastic deformation due to dislocation slip ceases. For all three metals, the theoretical threshold stress tracks the apparent trend of the increasing measured flow stress with the decreasing measured subgrain diameter.

In addition, we have shown only those flow stresses measured at the slowest strain rate reported by Varma, 0.01/minute. If Varma's data had been measured at a slower strain rate, one would expect the measured flow stresses to be closer the threshold flow stress of the material.

7. DISCUSSION

The theoretical predictions for active slip-plane spacing and flow stress are consistent with the experimental observations. This agreement between theory and experiment indicates that the theory accurately approximates the dislocation slip and extension that produces plastic deformation in FCC metals.

Consequently, it appears that many factors governing plastic deformation are significantly less important than the friction stress and the extension of dislocations. For instance, slip-plane misalignment with the maximum shear stress is not addressed. The anisotropic stiffness of the crystal lattice is not addressed. The complicated attractive and repulsive interactions of dislocations is not addressed except in the pile-ups. The dissociation of dislocations into partial dislocations in the low stress regions of the channels is not addressed. The random nature of barrier formation is not addressed. The effects of grain boundaries on stress fields are not addressed. Finally, subgrain formation is a multidimensional process, not limited to the simple geometry described here.

In spite of all these potential deficiencies, the approximate theoretical relationships developed here are apparently representative of the process. Moreover, these relationships are posed in terms of known or measurable fundamental parameters of the material. As such, these approximate relationships are advanced as completely theoretical expressions, based on first principles, for the equilibrium spacing of dislocation microstructure in a material and its threshold flow stress.

However, because of their approximate nature, these relationships must be employed with care. The active slip-plane spacing relationship is valid only when the shear stress is large

enough to produce spacing less than the initial grain size. In addition, the flow stress relationship is not applicable to plastic deformation governed by diffusion-driven vacancy motion. Moreover, these theoretical relationships are applicable only when the friction stress and dislocation extension are the dominant energies in the process of plastic deformation.

It is reassuring to note that this study's threshold flow stress relationship is based on dislocation extension. It is widely accepted that many materials exhibit a flow stress that evolves proportionally to the square root of dislocation density.(Hertzberg, 1976) This observation may be helpful in developing the rate equations governing the evolution of slip-plane spacing, dislocation density and flow stress. Because the flow relationship developed here is an equilibrium relationship, it is inappropriate to advance any conclusions about observed evolving dislocation densities that are in part driven by kinetics.

However, these equilibrium relationships should be viewed as approximate expressions for the combination of parameters that arrest plastic deformation. Said differently, these relationships should be used to construct the zero rate conditions in the state equations governing the kinetics of plastic deformation.

Because of the approximate nature of these equilibrium plasticity relationships, their ultimate value may not lie in their precise prediction of active slip-plane spacing and flow stress. Rather, the mathematical form of these relationships might be very valuable in constructing empirical engineering approximations that are representative of the plastic response of rather complicated alloys.

More specifically, it is possible that these equilibrium relationships may be applied to particulate second phase and solid solution FCC alloys. Generalizing the notion of the friction

stress, to describe the total energy expended to move a dislocation through a lattice containing impurities and/or small second phase particles, extends the applicability of these relationships to some alloys. The flow stress data for nickel in the previous section was measured on Nickel 200, a mild alloy.

In conclusion, approximate relationships describing the equilibrium conditions for plastic deformation through cross-slip in FCC metals have been developed. These results appear in the form of stress-strain relationships, where the strain appears as increments of plastic shear strain. Because the virtual work approach that produced these equilibrium plasticity relationships also reproduced the classical elastic equilibrium stress-strain relationships, these plasticity relationships are viewed as fundamental relationships governing plastic deformation in FCC materials.

8. REFERENCES

- Christensen, R.M., Mechanics of Composite Materials, Wiley and Sons, New York, 1979, pp. 32-37.
- Davidson, D., Private communication, September 1997.
- Eshelby, J.D., Frank, F.C., and Nabarro, F.R.N., "The Equilibrium of Linear Arrays of Dislocations," Phil. Mag., Vol. 42, 1951, p. 352.
- Eshelby, J.D., Frank, F.C., and Nabarro, F.R.N., "The Equilibrium of Linear Arrays of Dislocations," Phil. Mag., Vol. 42, 1951a, p. 357.
- Fung, Y.C., Foundations of Solid Mechanics, Prentice Hall, Englewood Cliffs, NJ, 1965, p. 285.
- Gurtin, M.E., "Variational Principles in the Linear Theory of Viscoelasticity," Archive Rational Mechanics and Analysis, Vol. 13, 1963, pp. 179-191.
- Hertzberg, R.W., Deformation and Fracture Mechanics of Engineering Materials, Wiley and Sons, New York, 1976, p. 94.
- Hodge, P., "A New Interpretation of the Plastic Minimum Principles," Quarterly of Applied Mathematics, Vol. 19, 1962, pp. 143-144.
- Honeycombe, R.W.K., The Plastic Deformation of Metals, 2nd Edition, Edward Arnold Ltd., London, 1984, p. 45.
- Honeycombe, R.W.K., The Plastic Deformation of Metals, 2nd Edition, Edward Arnold Ltd., London, 1984a, p. 12.
- Kachanov, L.M. "Variational Methods of Solution of Plasticity Problems," PPM - Journal of Applied Mathematical Mechanics, Vol. 3, 1959, pp. 880-883.
- McClintock, F.A. and Argon, A.S., Mechanical Behavior of Materials, Addison-Wesley, Reading Massachusetts, 1966, p. 149.
- Mugrahbi, H., "The Long-Range Internal Stress Field in the Dislocation Wall Structure of Persistent Slip Bands," Phys., Stat., Sol. (a), Vol. 104, 1987, pp. 107-120.
- Mugrahbi, H., "The Long-Range Internal Stress Field in the Dislocation Wall Structure of Persistent Slip Bands," Phys., Stat., Sol. (a), Vol. 104, 1987a, p. 117.
- Mura, T., Micromechanics of Defects in Solids, Kluwer Academic, Boston, 1987, p. 199.

- Nemat-Nasser, S. and Hori, M., Micromechanics: Overall Properties of Heterogeneous Materials, North-Holland, Amsterdam, 1993, pp. 27-33.
- Pian, T.H.H., "On the Variational Theorem for Creep," Journal of Aeronautical Science, Vol. 24, 1957, pp. 846-847.
- Pian, T.H.H., "Creep Buckling of Curved Beams Under Lateral Loading," Proceedings 3rd U.S. National Congress on Applied Mechanics, 1958, pp. 649-654.
- Raj, S.V., Iskovitz, I.S., and Freed, A.D., Unified Constitutive Laws of Plastic Deformation, Eds. A.S Krausz and K. Krausz, Academic Press, San Diego, 1996, pp. 344-439.
- Raj, S.V., Iskovitz, I.S., and Freed, A.D., Unified Constitutive Laws of Plastic Deformation, Eds. A.S Krausz and K. Krausz, Academic Press, San Diego, 1996a, p. 383.
- Raj, S.V., Iskovitz, I.S., and Freed, A.D., Unified Constitutive Laws of Plastic Deformation, Eds. A.S Krausz and K. Krausz, Academic Press, San Diego, 1996b, p. 384.
- Rao, J.G. and Varma, S.K., "The Effect of Grain Size and Strain Rate on the Substructures and Mechanical Properties in Nickel 200," Metallurgical Transactions, Vol. 24A, November 1993, pp. 2559-2568.
- Sanders, J.L., Jr., McComb, H.G., Jr., and Schelchte, F.R., "A Variational Theorem for Creep with Applications to Plates and Columns," NACA Report 1342, 1958.
- Sestak, B. and Seeger, A., "The Relationships Between the Work-Hardening of B.C.C. and F.C.C. Metals," Phys. Stat. Sol. (b), Vol. 43, 1971, pp. 433-444.
- Shankaranarayan, H., and Varma, S.K., "Strain-Rate and Grain-Size Effect on Substructures and Mechanical Properties in OFHC Copper During Tension," Journal of Material Science, Vol. 30, 1995, pp. 3576-3586.
- Sil, D. and Varma, S.K., "The Combined Effect of Grain Size and Strain Rate on the Dislocation of Substructures and Mechanical Properties in Pure Aluminum," Metallurgical Transactions, Vol. 24A, May 1993, pp. 1153-1161.